



**NANYANG
TECHNOLOGICAL
UNIVERSITY**

**MOVING BACKSCATTER TO
ENHANCE THE VISIBILITY OF
UNDERWATER OBJECT**

ZHANG HAO

**SCHOOL OF ELECTRICAL AND ELECTRONIC
ENGINEERING**

2016



**NANYANG
TECHNOLOGICAL
UNIVERSITY**

**MOVING BACKSCATTER TO
ENHANCE THE VISIBILITY OF
UNDERWATER OBJECT**

ZHANG HAO

SCHOOL OF ELECTRICAL AND ELECTRONIC ENGINEERING

**A DISSERTATION SUBMITTED IN PARTIAL FULFILMENT OF
THE REQUIREMENTS FOR THE DEGREE OF
MASTER OF SCIENCE IN COMMUNICATIONS ENGINEERING**

2016

Contents

Abstract.....	i
Acknowledgement	ii
Abbreviations.....	iii
List of Figures	iv
List of Tables.....	vi
1 Introduction	1
1.1 Background	1
1.2 Motivation	2
1.3 Objective and Specifications	3
1.4 Major Contribution of the Dissertation	3
1.5 Organization of the Dissertation.....	4
2 Literature Review.....	6
2.1 Underwater Optical Model	6
2.1.1 Light Absorption of Underwater Imaging System.....	7
2.1.2 Light Backscatters of Underwater Imaging System	8
2.1.3 The Impact of Artificial Light	9
2.1.4 Mathematical Formation of Underwater Optical Model	10
2.2 Physical Model-Based Underwater Imaging.....	11
2.3 Image Processing-Based Underwater Imaging.....	13
3 Enhancing Underwater Objects by Decomposition, Dehazing and Fusion	16
3.1 Image Decomposition.....	16
3.2 Dehazing and Color Correction for Illuminance Component.....	18
3.2.1 Global Underwater Background Light Estimation	18
3.2.2 Transmission Map Estimation	20
3.2.2.1 Coarse Estimation.....	20

3.2.2.2 Transmission Map Refinement.....	23
3.2.2.3 Transmission Map Enhancement.....	25
3.2.2.4 Enhanced Transmission Map for Each Color Component.....	27
3.2.3 Dehazing and Color Correction.....	29
3.3 Color Correction for Reflectance Component.....	30
3.4 Fusion Process.....	32
3.4.1 Weights of the Fusion Process	32
3.4.2 Multi-scale Fusion Process	34
4 Comparison, Evaluation and Analysis.....	37
4.1 Measurements of Underwater Imaging Performance	37
4.1.1 Basic Evaluation Index for Underwater Imaging Performance	37
4.1.2 Underwater Image Quality Metrics	40
4.2 Experiment Results and Evaluations	44
4.2.1 Basic Evaluation Measurements among Different Methods.....	44
4.2.2 UIQM Measurement among Different Methods	52
5 Conclusion and Recommendations	59
5.1 Conclusion.....	59
5.2 Further work.....	59
Bibliography	61

Abstract

Underwater vision enhancement via backscatter removing is widely used in ocean engineering. With increasing ocean exploration, underwater image processing has drawn more and more attention due to the important roles of video and image for obtain information. However, due to the existence of dust-like particles and light attenuation, underwater images and videos always suffer from the problems of low contrast and color distortion. In this thesis, we analyze the underwater light propagation process and propose an effective method to overcome the backscatter problem.

Our method is based on the underwater optical model and image fusion. It mainly contains three steps, first, we decompose input image into reflectance and illuminance components; second, we utilize color correction technology and dehazing technology to handle these two components separately; finally, in order to rebuild result well, we applied the Gaussian and Laplacian pyramids based multi-scale fusion to reconstruct the target image while exposedness, saliency maps are utilized as weights to assist the fusion task.

The experimental results show that our proposed method is able to greatly improve the quality of distorted underwater images. By introducing the underwater image quality metric measurements, we also analyze the intrinsic information and objective feature indexes of restored images via different methods. In general, our proposed method outperforms state of the art among sets of test images captured in different water environments and is demonstrated to be well-performed and effective.

Acknowledgement

The whole work proposed in this thesis cannot be completed without the professional instructions and support from my supervisor, Associate Professor, Lap Pui Chau. His tireless guidance has helped me grow a lot throughout my all Masters study. I greatly appreciate his patience and kindness. Here, I want to express my sincere thanks to him.

My senior, Research Assistant Liu Hui also helped me a lot in my research work. She gave me many study materials and precious resources. Her advices have inspired me a lot. The academic communication experience with her in the lab was so precious.

There are also many others who have given me a hand during my study. Among them, especially I would like to thank Yang Xiwen, Zhang Qifan and Wu Xianzhe for their help and accompany.

For my beloved family standing by me all the time, I will always be grateful and pray for them.

Abbreviations

SNR:	Signal-to-noise ratio
WCID:	Wavelength compensation and image dehazing
ARC:	Automatic red-channel restoration
DCP:	Dark channel prior
ACE:	Automatic color enhancement
SCB:	Simplest color balance
WB:	White balance
HE:	Histogram equalization
CLAHE:	Contrast-limited adaptive histogram equalization
CLAHS:	Contrast-limited adaptive histogram specification
QTS:	Quad-tree subdivision
MSE:	Mean square error
OTS:	Optimal transmission estimation
DCR:	Dynamic compression range
IGF:	Image guided filtering
GLPF:	Gaussian low-pass filtering
STD:	Standard deviation
AG:	Average gradient
GPD:	Gaussian pyramid decomposition
LPD:	Laplacian pyramid decomposition
UICM:	Underwater image colorfulness metric
UISM:	Underwater image sharpness metric
UIConM:	Underwater image contrast metric
UIQM:	Underwater image quality metric
EME:	Enhancement measure estimation
EMEE:	Measure of enhancement by entropy
logAMEE:	Logarithmic assessment by EMEE

List of Figures

1.1 Dissertation layout	4
2.1 Light attenuation of different color component	7
2.2 The physical mode of light propagation underwater	8
3.1 The general procedures of objects visibility enhancement process	16
3.2 Image decomposition result	18
3.3 Choosing background light from proper image block	20
3.4 An example of the transmission function	22
3.5 Coarse transmission map generated by general dark channel prior	23
3.6 Transmission map refinement via image guided filtering	24
3.7 Enhanced transmission map	26
3.8 Comparison of three transmission maps	27
3.9 Display of each color channel of an image	28
3.10 The transmission map of each color component	29
3.11 The processed result of illuminance component	30
3.12 The processed result of reflectance component	31
3.13 Luminance weight maps of two image components	33
3.14 Saliency weight maps of two image components	33
3.15 Exposedness weight maps of two image components	34
3.16 Normalized weight maps of two image components	35
3.17 The final output image via naive fusion process	35
3.18 The final output image via multi-scale Gaussian and Laplacian fusion process	36
4.1 RGB color space model and an example of image mapping in this color space	39

4.2 An example of edges detection of restored image	39
4.3 UICM example of original image and restored image	42
4.4 UISM example of original image and restored image	43
4.5 UIConM example of original image and restored image	43
4.6 The set of images chosen to evaluation and comparison	45
4.7 Results on diver image via different methods	45
4.8 RGB color space mapping of different restoration methods on diver image	47
4.9 Edge information of different restoration methods on diver image	48
4.10 Results on open scene image via different methods	49
4.11 RGB color space mapping of different methods on open scene image	50
4.12 Edge information of different restoration methods on open scene image	50
4.13 Results on fish image via different methods	51
4.14 RGB color space mapping of different restoration methods on fish image	52
4.15 Edge information of different restoration methods on fish image	53
4.16 Another set of images chosen to evaluation and comparison	53
4.17 Results on diver image (2) via different methods	54
4.18 Results on shoal image via different methods	56
4.19 Results on shoal image (2) via different methods	58

List of Tables

3.1 Comparison of three transmission maps via STD and AG	26
4.1 Statistic values of UICM for diver image	42
4.2 Basic visibility recovery coefficient of diver image	46
4.3 Basic visibility recovery coefficient of open scene image	49
4.4 Basic visibility recovery coefficient of fish image	51
4.5 Underwater image colorfulness metric (UICM) results of diver image (2)	55
4.6 Underwater image quality metric (UIQM) results of diver image (2)	56
4.7 Underwater image colorfulness metric (UICM) results of shoal image	56
4.8 Underwater image quality metric (UIQM) results of shoal image	57
4.9 Underwater image colorfulness metric (UICM) results of shoal image (2)	58
4.10 Underwater image quality metric (UIQM) results of shoal image (2)	58

Chapter 1

Introduction

1.1 Background

With the rapid development of social productivity and improvement of technology, the limited space and resources of land cannot satisfy the gradually increasing requirements of human. However, ocean occupies 71% superficial area of earth, which contains huge energy, luxuriant mineral resources and biological resources. In order to maintain the survival and development of human, people start to explore the ocean. As ocean exploration increased, the area of underwater image processing has drawn more and more attention over the last years, since video and image are the important ways to obtain and record information nowadays, and the implementation of video and image processing becomes more and more wide. But taking videos and images is easily affected by the environment factors, such as light condition, air humidity and quality, haze and so forth, which cause the existence of information loss and different degree of degradation in different environments. For underwater environment, because of its complexity and particularity, videos and images taken under such condition often show extremely serious distortion and noise, which can not be used to do analysis and measurement directly. So, underwater image processing plays a significant role in ocean engineering.

It is known that acquiring distinct and high contrast underwater images is an important task for ocean engineering and their quality also acts as a crucial role in different scientific researches, such as navigation of autonomous underwater vehicles, monitoring marine organism, taking census of popularities of marine organism, analyzing the geological or biological environments, object recognition and so forth. However, challenges associated with capturing images underwater have been difficult to overcome, due to the existence of haze and color casting. Since the

haze is caused by light, which is deflected and scattered by dusk-like particles underwater while color casting due to varying light attenuation degrees of different light wavelengths. In general, color cast and light scattering cause the color derivation and contrast degradation in images and videos acquired underwater.

1.2 Motivation

Image enhancement methods for underwater degradation images usually include exploring the underwater optical model and compensating the bad effects caused by water and particles, or merely using image processing methods to restore the performance of distorted images. The state-of-arts are mostly designed for single image restoration, since multi-images input may limit the implementation range and slow down the processing speed. Intuitively, in order to handle this issue well, the underwater optical model should be studied and explored at first. Among various underwater imaging algorithms, the representation method, WCID [1], gives a comprehensive underwater optical model, in which the light propagation path, light attenuation ratio of different color channel, vertical and horizontal depth of underwater environment, artificial light effects and etc. are taken into consideration. This method is totally based on physical model and achieves excellent for some underwater backscatter issues, however, its estimation process is complex and time-consuming, which is hard to practicability, but it provides a full-scale analysis of underwater environment. For image processing based method, Ancuti et al. proposes a fusion based method, which fuses the processing results by color constancy algorithm and histogram equalization algorithm, it also generates good results for many different underwater environments, however, because it only uses the technique of image processing and ignores the features of underwater environment, so its results suffer from more or less slight haze and information loss as well as over-enhancement drawbacks. In order to solve the underwater distorted image issue well, the advantages of both two types of underwater imaging techniques should be combined and new method should be proposed.

1.3 Objective and Specifications

The target of this research is developing an improved physical model-based underwater image restoration method to remove backscatters and enhancing the visibility of underwater objects.

The task includes the following parts:

- Studying and analyzing the principles and mechanisms of underwater objects which suffer from backscatter effect in various degrees, and exploring the underwater optical model.
- Exploring the light absorption, contrast attenuation and backscatter effects compensation technology of underwater issue according to the physical properties of underwater optical model.
- Introducing image decomposition technology to separate the task into different parts, and executing different specific methods to handle them separately, finally multi-scale weighted image fusion technology is utilized to reconstruct the restored results.
- Implementing the designed underwater objects visibility enhancement method on different testing images captured in various water environments.
- Comparing performances and results among different methods, analyzing the advantages and limitations.

1.4 Major Contribution of the Dissertation

The major contributions of this thesis are: an effective and efficient underwater objects visibility enhancement method is designed for distorted and attenuated underwater images and videos to estimate and rebuild the correct color, scene depth, contrast and details information. It introduces and implements several state-of-art underwater imaging algorithms as well as utilizes thorough and comprehensive image quality metric measurements to analyze the performance of our method and state of the arts. Moreover, the state-of-arts is generally divided into two parts, one is based on underwater optical model, i.e., physical model method while another is

based on image processing, which is focus on compensating the color casting and enhancing the degraded contrast by applying different image process methods like color constancy, histogram equalization and etc. However, such physical model based methods is limited in different types of water environments, since the situations like the elements and contents of dust-like particles and water qualities are various among different water environments. Meanwhile, the image processing based methods show wide implementation range of different water environment and are able to generate proper restoration results, but some drawbacks like slight haze, unclear details are still existing, making it hard to obtain excellently clear images with high dynamic compression range, good color performance and great contrast. Our method combines the advantages of physical model based methods and image processing based methods, in which we decompose image into different parts to represent their intrinsic features, then utilizing different restoration methods for each component separately and fusion technology is introduced to rebuild the final results. And the final results of proposed method are close to or even slightly better than the state of the arts.

1.5 Organization of the Dissertation

The dissertation is arranged by below layout:

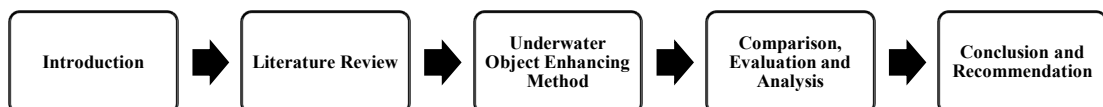


Figure 1.1 Dissertation layout

Chapter 1 introduces an overview of the general concepts of the underwater imaging backgrounds as well as the motivation behind the proposal of new algorithm and the objective of the dissertation.

The review of related works is stated in chapter 2, the issue suffered in this domain and different technologies and methods are analyzed, which includes underwater optical model description, physical model-based underwater imaging and image

processing-based underwater imaging.

Chapter 3 is focused on proposed algorithm, including the general ideas, modification procedures and improved underwater video and image restoration method.

The experiment results evaluation, comparison and analysis are proposed in chapter 4. It covers the completed procedures of underwater image processing tasks. Performance comparisons of different methods and the methods analysis are also proposed in this chapter.

In chapter 5, it comes to the conclusion and summary of this thesis as well as recommendation of future work.

Chapter 2

Literature Review

In this chapter, the related theories and technologies of underwater image processing research will be introduced. It includes the underwater optical model, physical model-based underwater imaging and image processing-based underwater imaging.

2.1 Underwater Optical Model

Underwater images often show color cast and contrast degradation, which is common physical phenomenon caused by the special light propagation environment. In general, images captured by underwater imaging system have two features [2]:

- (1) Color fading caused by light absorption [3]. The absorption of light by water shows its selective feature for different areas of light spectrum, since the density of water is approximate 800 times of that of air. The energy of light decrease with the increase of the depth of water. Meanwhile, water molecule can absorb some light energy. Color depends on wavelength, along with the wavelength decrease, color fade away.
- (2) Low visibility and blur of image caused by light attenuation [3]. The decay of light radiation is mainly caused by absorption, which leads the decrease of luminous energy and scattering, which leads light path direction change in the water. It impacts the whole performance of underwater imaging system.

The two features are the main issues, which cause the underwater images degradation. However, the existence of artificial light also has impact on the underwater images for some cases.

2.1.1 Light Absorption of Underwater Imaging System

In marine environment, assuming that the air light is parallel light and arrives at the water surface vertically, some of light energy is reflected into air by the water surface, while the residual light transmission underwater can be separated into two parts, one is the light travelling from air environment to the objects in water, i.e., vertical direction, another is the reflectance from objects to be captured by camera in the horizontal direction. Unlike light propagation in the air environment, where each color component of light suffers almost the same degree of absorption, since the density of water is much larger than that of air, it shows different absorption properties for different light wavelengths, so the color of underwater images is usually distorted. Normally, red component disappears firstly underwater because of its longest wavelength, i.e., red component always has the minimum energy, while blue light, with shortest wavelength, transmits the longest path under water. Thus, underwater images are often dominated by blue color.

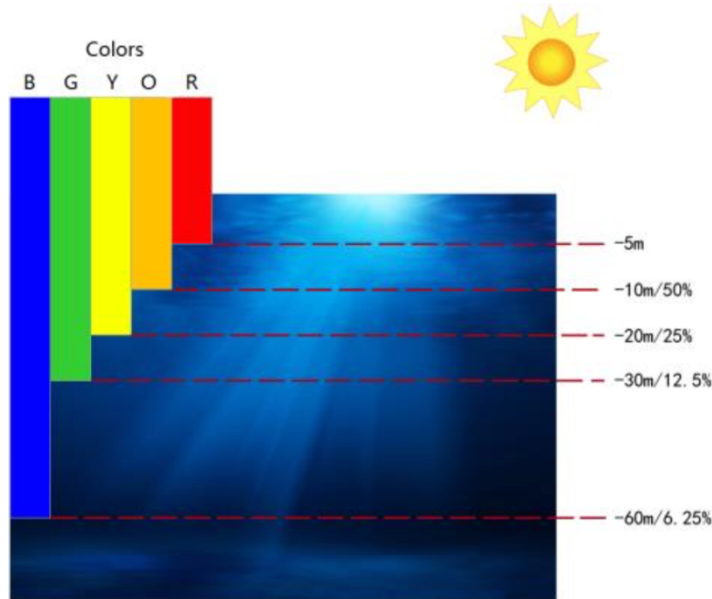


Figure 2.1, light attenuation of different color component [2].

As shown in the figure, the red color component of light is absorbed and disappears firstly, followed by orange and yellow color components, while green and blue components can reach the much deeper distance than other color components. In

general, we only consider the three primary colors, i.e., red, green and blue. Under normal conditions, the blue component can transmit the deepest distance due to its shortest wavelength, following by the green component, while red component shows weakest property of transmission in the water.

2.1.2 Light Backscatters of Underwater Imaging System

However, not only the water itself has impact on the light but also the dust-like particles, such as the organic matter (micelle, germ, plankton, etc.) and inorganic substance (quartz sand, clay mineral, metallic oxide, etc.), can cause low SNR, low contrast ratio and blurred details of image in underwater heterogeneous light field [2]. Since light beams travels with a straight-line propagation path in water, a portion of light is likely to meet with these suspend particles. These particles tend to absorb and scatter the light beams, which contributes to enlarge the contrast degradation of captured images as well as color cast amplification. Further the light scattered by particles, because of the absence of blackbody radiation, propagation process will disperse light beams into homogeneous background light, which further causes the haze underwater.

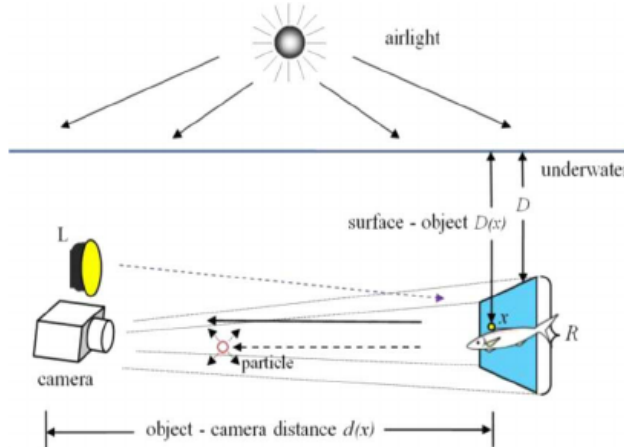


Figure 2.2, The physical model of light propagation underwater [1].

As shown in the figure, light firstly travels from air to the underwater objects at point x by traveling a vertical distance $D(x)$, then light reflected propagates a distance

$d(x)$ from objects to the camera. Normally, images captured by camera is combined with two parts: one is the multi-scattering background light and another is direct transmission of reflected light [1]. Moreover, different underwater environments also show different attenuation and backscatter features of light, which causes the captured underwater images perform various degrees of contrast reduction and color cast. Assuming that the water environment can be generally classified into three types, marine environment, lacustrine environment and fluvial environment. Using the marine environment as an example, it is can be further classified into different categories according to the different water qualities and John et al. [1] classifies marine environment into three types, oligo-water, meso-water and eutrophic-water.

2.1.3 The Impact of Artificial Light

Due to the energy loss through light propagation under water, the light energy becomes lower and lower when depth increases, which objects under deep water are darker and color distortion is more serious than those in swallow water. In this situation, it is hard for the camera to capture a distinct image, thus the artificial light is needed to compensate the energy loss of natural light to increase the lightness of underwater objects and guarantee the camera to take clear images. However, the absorption of water and backscatters of suspend particles also have impact on the artificial light, since the artificial light often is emitted from somewhere near the camera to the objects and is reflected from the objects propagates toward the camera, the artificial light suffers two times energy loss of each color component and backscatters along the distance between camera and objects. What's more, although artificial light may contribute to compensate the color distortion effect. The color of artificial light also has to be taken into consideration, since if the artificial light contains different color components of light compare to the natural light, it may cause the non-collinear color distortion, which makes the problem more complex.

2.1.4 Mathematical Formation of Underwater Optical Model

According to the Lambert-Beer's law, the reduction of light intensity through propagation is mainly related to the properties of material and the reduction feature follows the exponential form [3]. The light intensity E at position x with distance $d(x)$ can be modeled as:

$$E(x) = E(0) \cdot e^{-c \cdot d(x)} \quad (2-1)$$

where c is the total attenuation coefficient of the material, which is also a measurement of energy loss of absorption and backscatter effects via a unit length of transmitting in such medium. So the coefficient c can be further decomposed to two factors, absorption coefficient a and backscatter coefficient b , then the equalization (2-1) can be rewritten as:

$$E(x) = E(0) \cdot e^{-a \cdot d(x)} \cdot e^{-b \cdot d(x)} \quad (2-2)$$

The backscatter coefficient b represents the super-position of scattering at all angles, using the volume scattering function $\beta(\theta)$ can express b as:

$$b = 2\pi \cdot \int_0^\pi \beta(\theta) \cdot \sin(\theta) d\theta \quad (2-3)$$

These parameters, a , b , c and β , depend on the location x and theoretically allow to predict light transmission property in water. However, taking different attenuation rates of light with different wavelengths underwater into consideration, the parameters are various for each color component, i.e., $c(\lambda)$, where $\lambda \in \{r, g, b\}$. And considering the propagation path of light in water and different features of different water types, the measurements are not sufficient to present light propagation underwater, a more comprehensive and computational model is needed. Simply, we only consider the total attenuation coefficient c .

Due to the similarity of hazy images and underwater images, they also have the similar formation. This model is widely used to represent hazy image [4]:

$$I(x) = J(x) \cdot t(x) + A \cdot (1 - t(x)) \quad (2-4)$$

where A is the global atmospheric light, $I(x)$ is captured image, $J(x)$ is the target radiance while $t(x)$ is transmission map, and $t(x) = e^{-c \cdot d(x)}$. However, water has

different absorption and backscatter features of light components, which causes each color component having various transmission feature and background light, so each component should be treated individually. And considering the vertical depth of scenes underwater and possible existence of artificial light, the overall mathematical formation of underwater optical model can be written as:

$$I_\lambda(x) = (J_\lambda(x) \cdot T_\lambda(x) + L_\lambda(x) \cdot t_\lambda(x)) \cdot t_\lambda(x) + A(\lambda) \cdot (1 - t_\lambda(x)) \quad (2-5)$$

where $\lambda \in \{r, g, b\}$, $I_\lambda(x)$ represent each color component of captured image, $J_\lambda(x)$ is the scene radiance, $L_\lambda(x)$ is the possible existence of artificial light, $A(\lambda)$ is the background light, $T_\lambda(x) = e^{-c(\lambda) \cdot D(x)}$ express the light attenuation in the vertical direction, i.e., vertical transmission and $t_\lambda(x) = e^{-c(\lambda) \cdot d(x)}$ is transmission map in the horizontal direction.

Thus, the task of underwater imaging is obtaining the scene radiance $J_\lambda(x)$ from observed image $I_\lambda(x)$, it is a extremely complicated issue, since all the right terms of equalization (2-5) are unknown and needs to be estimated. In the next sub-sections, two kinds of underwater imaging methods are introduced to deal with this issue.

2.2 Physical Model-Based Underwater Imaging

Clear images with high quality are the most important part for oceanic engineering. The physical model-based imaging is also the most common and effective method to restore and enhance the performance of underwater images, which according to the processes of light attenuation and backscatters in the water, trying to compensate and counteract the poor effects reversely. For instance, some researchers try to solve this problem through modifying physical model of defogging methods due to the similarity between dehazing and underwater imaging. The main challenges of physical model-based methods are the estimation of underwater background light, transmission map and depth of scenes according to the mathematical formation of light attenuation model. The background light is considered to be homogeneous because of the scattering of dust-like particles, while transmission map is a measurement of distance from camera to objects and the depth mainly contributes to

color distortion.

According to the researches of oceanic water and river water features, the physical model of underwater environment can be established and used to handle distorted and degraded underwater images. Chiang et al. [1] analyze the features of underwater environment and modify the physical model of dehazing to make it more suitable for underwater situation. Since physical model based restoration methods is similar to dehazing process, the author designs the solution of underwater image enhancement by wavelength compensation and dehazing (WCID). After separating the water environment into three types and mathematically defining their formations, the author adds these formations into physical model, the dark channel prior is utilized to estimate the background light and transmission map, image matting method is utilized to refine the transmission map, image segmentation method plays a role of removal of artificial light and the least squares solution is used to derive the vertical depth of objects. Although John et al. achieves great result though the proposed method, this method is complicate and hard to implementation because of its high computer complexity and redundant algorithm procedure.

In contrast to WCID method, Adrian et al. [5] propose a faster automatic red-channel underwater image restoration method (ARC), which considers the fastest attenuation of red color component of light and utilizes a modified model to achieve more compensation on red component. Instead of estimating the dark channel, the author constructs a model, which is similar to DCP, to obtain transmission map of red channel. Then the background light is chosen as the brightest pixel in its red channel, and the transmission map also can be derived under the red channel hypothesis. After that, the author incorporates color correction by defining the vertical transmission and weighted water-light value. The experiment results show that this method performs well on some test images.

Zhen et al. [6] propose a region-specialized method for underwater image restoration, they treat the background light is inhomogeneous and introduce the idea of bright channel prior. Since additional sources except the parallel background light will

cause pollution to the underwater optical environments, making it inhomogeneous. In this condition, the popular image processing methods based on the assumption of the homogeneous ambient light are weak or even futile, while region-specialized method is able to avoid the drawbacks and shows great performance by estimating and eliminating the abundant sources.

Instead of constructing a new or modified physical model, some researchers handle the challenges of underwater imaging by combining classical dehazing physical model and other mathematical methods. For instance, Lu et al. [7] introduces a guided trigonometric bilateral filter to improving the performance of transmission map estimation and contrast enhancement, and the automatic color correction method is utilized to correct the color distortion. Zhao et al. [8] explore underwater background color has relationship with optical properties of water, and build an algorithm to derive water properties from background color according to underwater image formation model. Experimental results show a good performance for underwater image.

2.3 Image Processing-Based Underwater Imaging

Despite the physical model based methods often achieve excellent result in specific situations, these methods are not able to generate great results for varieties of underwater environments all the time. In order to design algorithms to handle the underwater images captured in different underwater environments and obtain relatively satisfied results, researchers alternatively explore image processing methods to solve the issues of underwater image.

Color constancy is the ability to measure objects' colors independent of the color of the light source [9], since underwater images often suffer the poor effect of color distortion which makes the image is dominated by one color component (green or blue) and indirectly reduce the contrast, it is able to use the concept of color constancy to correct the color cast issue. According to the gray world assumption

[10], the mean of each color component of underwater image should be approximately same, thus related color correction methods, such as automatic color enhancement (ACE) [11] and simplest color balance (SCB) [12], are introduced to process this issue. However, these methods are able to correct the color cast problem, but they can not solve contrast degradation well caused by dust-like particles. Histogram equalization (HE) algorithms [13, 14] are effective methods with low computational complexity and great performance, which stretch the histograms of image to improve the dynamic range compress and map the whole display area to achieve contrast enhancement, but these methods often cause over-enhancement, amplify the noise and show poor effect on color correction.

Due to the drawbacks of single image processing methods, some relatively complicated methods are proposed. Ancuti et al. [15] propose a fusion-based restoration method to deal with underwater images. This method uses two inputs as the resources of fusion, one is white balance result and another is histogram equalization result, then four weight maps are generated to compute the normalized weight map, and follows by the Gaussian pyramid-based fusion process. Because of over-saturation and color aberration for some test images, the author modifies and proposes an improved fusion algorithm [16], which obtains excellent performance.

Meanwhile, Fu et al. [17] proposes a retinex-based approach to deal with the underwater issues. Retinex theory [18] is constructed as the objects perceptual model of human visual system, which performs well on image enhancing domain. Combining with the gray-world assumption, Fu transforms image to *Lab* color space and initially separates *L* layer into reflectance (*R*) and illumination (*I*) using the concept of retinex theory, then an alternating direction optimization algorithm is introduced to calculate and update *R* and *I* iteratively, and the contrast-limited adaptive histogram equalization (CLAHE) method is utilized as post-processing to enhance the global performance, however, the performance of this method is not distinct, color cast and contrast degradation still exist.

Ghani et al. [19, 20] propose a dual-image Rayleigh-stretched contrast-limited

adaptive histogram specification (CLAHS) method, which integrates global and local contrast correction. It separates images according to the middle point of histogram, stretches regions towards upper and lower directions and CLAHS is utilized to do local contrast correction, after that, stretching each component of image according to Rayleigh distribution in the HSV color space. This method achieves great result in bluish underwater images, but do not always keep good performance for different test images, and it also suffers from higher level of information loss.

Chapter 3

Enhancing Underwater Objects by Decomposition, Dehazing and Fusion

In this chapter, a novel method based on underwater optical model for underwater object visibility enhancement is proposed. The input image is firstly decomposed to reflectance and illuminance. Then color correction and dehazing methods are utilized to process each component separately, according to their specific features. Finally, we calculate the weights of two components and apply an efficient image fusion method to obtain the enhanced image.

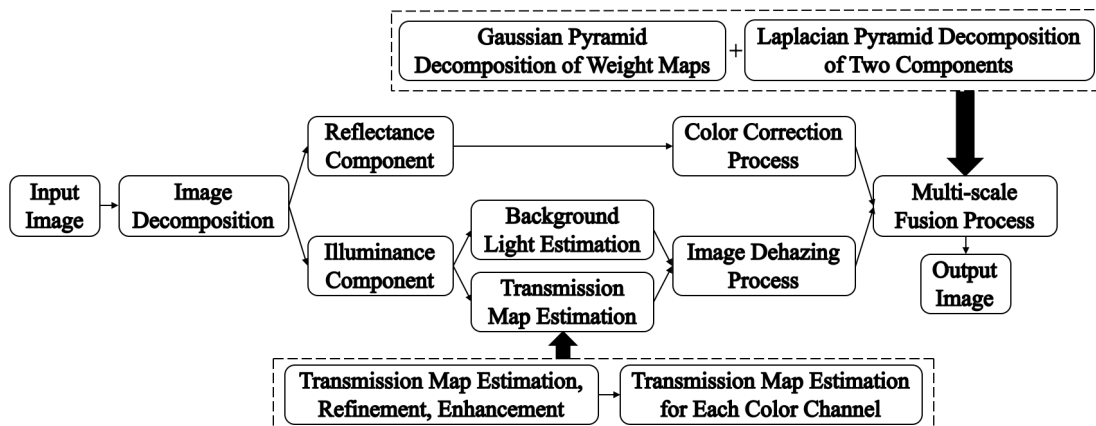


Figure 3.1, The general procedures of objects visibility enhancement process

3.1 Image Decomposition

As an important pre-process method, image decomposition is widely used in video and image processing to separate images and videos into several parts and then execute different processing methods according to their features. Image decomposition methods like wavelet transform and weighted decomposition are most popular methods in this domain. For the case of underwater image processing, we

want to separate images into several parts and each part contains a specific features obtained from original image, such as illumination and reflectance. Wavelet transform method is widely used in image denoising and enhancement, however, for this case, it is not suitable because it is time consuming and can not extract the features we want from the original image. Thus, we introduce a weighted image decomposition method, which separates original image into two parts, one expresses the illumination component of image while another expresses the reflectance component of image.

Since the process of camera captures scenes is based on the luminance of light which is reflected from objects or scenes to camera. For a clear environment, the radiance intensity of scenes spread widely in the display range, which makes captured image shows good contrast information and mean value is closed to middle gray according to gray world assumption. However, for the situations with hazy case, the reflectance would be distorted. For this situation, in order to obtain accurate luminance and reflectance, we should derive the reflectance component and illumination component by decomposing original image. Firstly, an image can be expressed as:

$$I_\lambda(x) = I_\lambda^R(x) + I_\lambda^I(x) \quad (3-1)$$

where $\lambda \in \{r, g, b\}$ represents each color component of image, $I_\lambda^R(x)$ is the reflectance component and $I_\lambda^I(x)$ is the illumination component.

$$I_\lambda^R(x) = \Upsilon \cdot I_\lambda(x) \quad (3-2)$$

$$I_\lambda^I(x) = (1 - \Upsilon) \cdot I_\lambda(x) \quad (3-3)$$

where Υ is a weighted parameter, which maintains bright areas remains brighter than dark areas and enhances the contrast of reflectance component to remove the backscatter effect from it as much as possible. So Υ can be derived by

$$\Upsilon = \xi \cdot \frac{I_\lambda(x)}{I_\lambda^{max}} \quad (3-4)$$

Where I_λ^{max} is the maximal pixel value of λ color channel, and ξ is a control parameter to determine the weight of reflectance component, and $\xi \in (0,1)$, if $\xi = 0$, the whole image is treated as illuminance component, while $\xi = 1$, the whole image is otherwise treated as reflectance component. For further image process, we consider that the backscatter effect only exists in the illuminance component, while

reflectance component only suffers from color distortion.

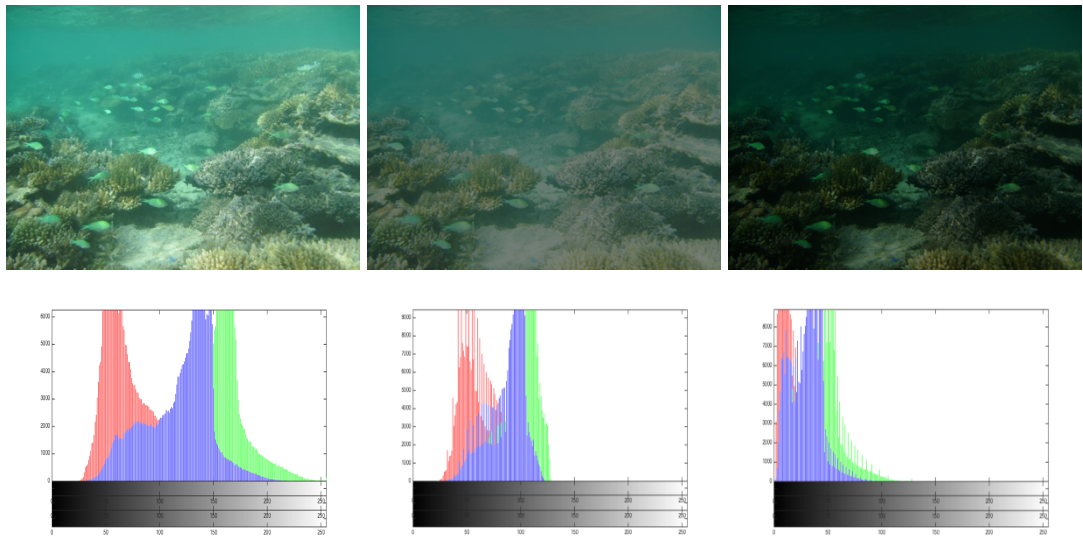


Figure 3.2, Image decomposition result, from left to right: original image and its corresponding histogram, illuminance component and its corresponding histogram, reflectance component and its corresponding histogram.

3.2 Dehazing and Color Correction for Illuminance Component

3.2.1 Global Underwater Background Light Estimation

Images of underwater scenes and objects are degraded and distorted by the turbid medium such as dust-like particles, and the different absorption features of water for light beams with different wavelength. The effect of light absorption often causes the color fading of captured objects and scenes, which makes objects and scenes become bluish and greenish, since the wavelengths of green and blue light are shorter than that of red light, where red light attenuates fastest in the water. Meanwhile, dust-like particles also produce part of color fading due to its absorption of light energy. So some objects captured underwater show bluish while others show greenish, since water environments of different areas are various, and contain different turbid medium. However, despite the part of light absorption of turbid medium, they mainly

contribute to contrast degradation by scattering and reflecting the light into different directions. In the absence of black-body radiation, this multi-scattering process makes light further becomes background light [1], and leads the objects and scenes to be covered by slight haze. This process is similar to the haze in the atmospheric environment.

Conventionally, in the atmospheric environment, among different estimation methods, the background light is considered to be homogeneous, and is often estimated as the brightest pixel or average value of the brightest area in the images, since a large amount of haze is more likely to cause bright color. For underwater environment, taking the color fading caused by light absorption into consideration, the background light is not white, i.e., pure haze, but bluish or greenish. However, the dust-like particles play a similar role as that in the atmospheric environment, so it is suitable to utilize the analogous ways to estimate the background light underwater, and the obtained background light also gives the intrinsic information of light absorption of different wavelengths.

In order to estimate the background light, an ideal way is to pick up a pixel or an area lies as the maximum depth with regard to the camera, since color distortion and contrast degradation are distance dependent. With distance increases, the haze is denser due to the scattering of turbid medium, which causes relatively brighter color. However, in this scheme, objects or scenes, which are brighter than the background light, may lead to an undesirable selection result. In order to obtain accurate result, this scheme should be eliminated. Since the variance of objects and scenes pixel values are lower with denser haze, we utilize a hierarchical searching method based on the quad-tree subdivision (QTS) [21] to execute this process. Firstly, the image is separated into four equal rectangular regions, then for each region, we compute the average value subtract the standard deviation values as shown below:

$$Score_l = \frac{1}{3N} \sum_{\lambda \in \{r,g,b\}} \sum_{x=1}^N I_l^\lambda(x) - \frac{1}{3} \sum_{\lambda \in \{r,g,b\}} \sqrt{\frac{\sum_{x=1}^N (I_l^\lambda(x) - \bar{I}_l^\lambda)^2}{N}} \quad (3-5)$$

Where $l = 1,2,3,4$ represents to the four image regions, N is the pixel number within the region, $I_l^\lambda(x)$ is the pixel value of x point of λ component of l region, \bar{I}_l^λ is the

average pixel value of c component of l region. After that, we select the region with the lowest variance, and divide it into four regions as done before. These processes are repeated till the size is less than the threshold, and normally we set this threshold to 100. Within the determined region, we calculate mean value vector as the final obtained background light and this vector can be considered as the approximately brightest value with the full image.

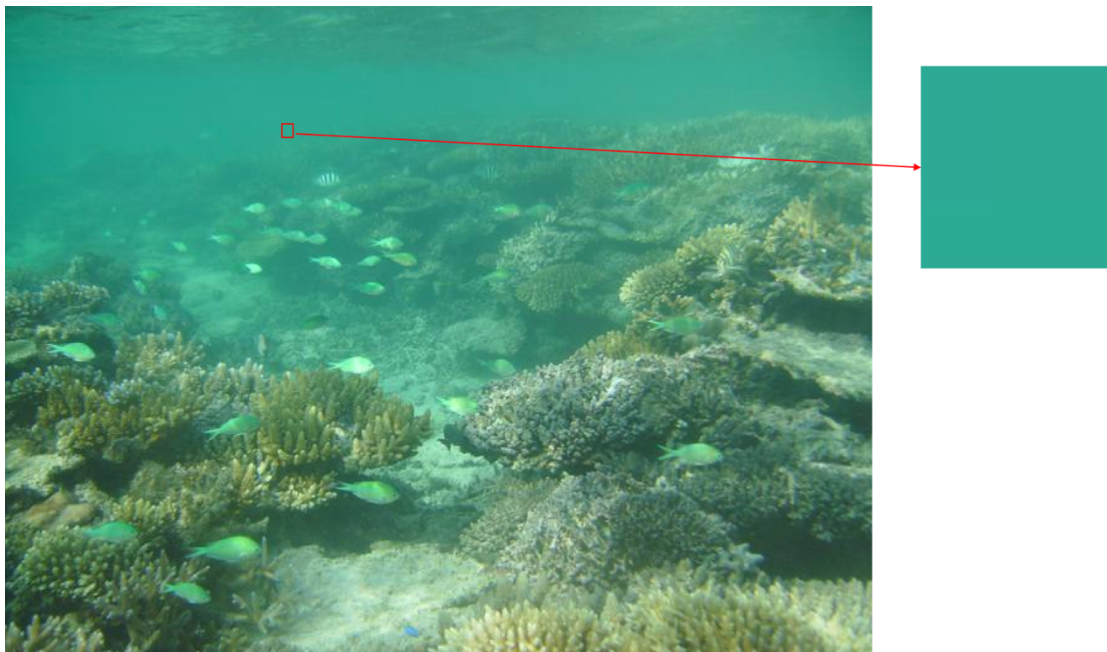


Figure 3.3, Choosing background light from proper image block

3.2.2 Transmission Map Estimation

3.2.2.1 Coarse Estimation

Assuming the background light is given, according to the underwater optical model formation in (2-5), in order to recover scenes or objects radiance from the captured image, we still need to estimate the $T_\lambda(x)$, $t_\lambda(x)$ and the effect of artificial light. However, for most case, especially in the swallow underwater environment, there is little effect of artificial light. Simply, we eliminate the impact of artificial light and derive the simplified model as:

$$I_\lambda(x) = (J_\lambda(x) \cdot T_\lambda(x)) \cdot t_\lambda(x) + A(\lambda) \cdot (1 - t_\lambda(x)) \quad (3-6)$$

Where $A(\lambda)$ is already known after background light estimation, we firstly consider $J_\lambda(x) \cdot T_\lambda(x)$ to be one part, denotes as $J_\lambda^T(x)$, then the formation can be written as:

$$I_\lambda(x) = J_\lambda^T(x) \cdot t_\lambda(x) + A(\lambda) \cdot (1 - t_\lambda(x)) \quad (3-7)$$

It has the similar format as hazy formation model and we can derive $J_\lambda^T(x)$ by estimating the transmission map in the horizontal direction, $t_\lambda(x)$. In such scheme, the transmission map estimation for dehazing in the atmospheric environment can be utilized to compute the transmission map of underwater case after some modifications, since both of these two environments are similar to each other.

Among many transmission map estimation methods, dark channel prior (DCP) assumption is excellent and effective, it is also used widely in solving the dehazing issue. The dark channel prior is based on the statistics of outdoor haze-free images [4]. The author finds that most of the local regions in the image which cover the scenes and objects, some pixels in at least one color channel have very low intensity values. However, there is no such phenomenon for hazy images, since these dark pixels become bright due to the effect of background light. According to discovery of dark channel prior, the dark pixels can provide the accurate estimation of haze transmission map, i.e., depth map. However, dark channel prior method often causes over-enhancement in local areas, especially for underwater images, since it only generates a transmission map for three color channels and does not consider the color fading and energy loss in the water, which make the transmission maps of each color channel are different.

To estimate the transmission map of each color channel more accurate, we choose an optimal transmission estimation (OTS) [21] method to prevent the over-enhancement and obtain optimized estimation. This method is a generalized DCP, and in the DCP, scene depth is considered to be local similar, and some pixels within the local area of at least one color channel is nearly to be zero. Since the backscatters due to dust-like particles tend to reduce the contrast of local area, inversely, the contrast information of a degraded area also seems to implicit the effect of backscatters. So the mean square error (MSE) is utilized to measure the contrast of local scene area. The MSE

contrast represents the variance of pixel values [22], which is given by:

$$\mathcal{C}_{MSE} = \sum_{x=1}^N \frac{(J_\lambda^T(x) - \bar{J}_\lambda^T)^2}{N} \quad (3-8)$$

where \bar{J}_λ^T is the average pixel value of $J_\lambda^T(x)$, N is the pixel amount within the local area B . By transforming the (3-4), we can derive the expression of $J_\lambda^T(x)$,

$$J_\lambda^T(x) = \frac{1}{t(x)} \cdot (I_\lambda(x) - A(\lambda)) + A(\lambda) \quad (3-9)$$

then \mathcal{C}_{MSE} can be rewritten as,

$$\mathcal{C}_{MSE} = \sum_{x=1}^N \frac{(I_\lambda(x) - \bar{I}_\lambda)^2}{N \cdot t(x)^2} \quad (3-10)$$

Considering the transmission value is locally same and MSE contrast is inversely proportional to the transmission value $t(x)$, which means the contrast of local area is greater with smaller $t(x)$. However, $t(x)$ can not be arbitrarily small because it may cause some pixel values of restored image out of the full dynamic range, and further lead information loss, as shown in Figure 3.4, only pixel values within $[\alpha, \beta]$ can be enhanced after mapping process, other pixels will be truncated. In general, choosing a larger transmission value is able to reduce the information loss, but contrast is enhanced by choose smaller transmission value.

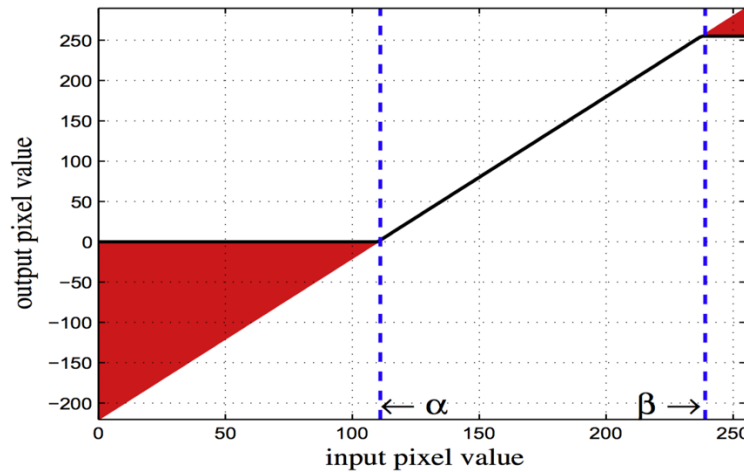


Figure 3.4, An example of the transformation function [21].

In Figure 3.4, the red regions represent the information loss due to the truncation of output pixel values, and input pixel values are mapped to output pixel values according to a transformation function. Thus, the transmission value of $t(x)$ can not be chosen arbitrarily, contrast enhancement and information loss reduction should be

taken into consideration at the same time. First, the contrast enhancement cost function, E_c and information loss cost function, E_i are designed and then minimize the two functions simultaneously, where contrast enhancement cost is defined as the negative sum of \mathcal{C}_{MSE} of all color channels and information loss cost is defined as the sum of square value of truncated pixel values.

$$E_c = - \sum_{\lambda \in \{r,g,b\}} \sum_{x=1}^N \frac{(J_\lambda^T(x) - \bar{J}_\lambda^T)^2}{N} = - \sum_{\lambda \in \{r,g,b\}} \sum_{x=1}^N \frac{(I_\lambda(x) - \bar{I}_\lambda)^2}{N \cdot t(x)^2} \quad (3-11)$$

$$E_i = \sum_{\lambda \in \{r,g,b\}} \sum_{x=1}^N \{(\min \{0, J_\lambda^T(x)\})^2 + (\max \{0, J_\lambda^T(x) - 255\})^2\} \quad (3-12)$$

Finally, for each local area B , the optimal transmission value $t(x)$ is estimated by minimizing the following function,

$$E = E_c + \gamma \cdot E_i \quad (3-13)$$

where γ is a weighted parameter to control the influence of information loss cost.



Figure 3.5, Coarse transmission map generated by general dark channel prior, left: illuminance component, right: corresponding coarse transmission map

3.2.2.2 Transmission Map Refinement

In sub-section 3.2.2.1, the transmission value is treated to be local constant of a block. However, the scene depths within each local area are vary spatially and block-based local constant transmission value is likely to yield block artifact, further to weaken the contrast of restoring image. In order to solve this problem, different methods have been proposed to refine the transmission map. Fattal [23] uses Gaussian-Markov random field model guided by original image to refine the

transmission map, but it is computationally intensive. He [4] uses the soft matting method to do the refinement, which is also time-consuming. Among different methods, image guided filtering [24] is an effective and efficient method to refine the transmission map, which also uses an input image as a guidance.

As described by He [4], transmission map refinement can be executed by solving a sparse linear system:

$$(\mathbf{L} + \lambda \cdot \mathbf{U}) \cdot t = \lambda \cdot \tilde{t} \quad (3-14)$$

where \mathbf{L} is matting Laplacian matrix, and \mathbf{U} is the identity matrix with the same size as \mathbf{L} , and λ is a regularization parameter. Since in image guided filter, its kernel has the similar form of the elements of matting Laplacian matrix, thus its elements can be represented by:

$$L_{ij} = |\omega|(\delta_{ij} - W_{ij}) \quad (3-15)$$

where $|\omega|$ is the number of pixels in a block, δ_{ij} is Kronecker delta, and W_{ij} is the guided filter kernel weight, which is defined as:

$$W_{ij} = \frac{1}{|\omega|^2} \cdot \sum_{k:(i,j) \in \omega_k} \left(1 + \frac{(I_i - \mu_k) \cdot (I_j - \mu_k)}{\sigma_k^2 + \tau} \right) \quad (3-16)$$

where μ_k is mean of I , σ_k^2 is variance of I , τ is the regularization parameter and I is the guidance image. Thus, the transmission map is refined by computing (3-14).

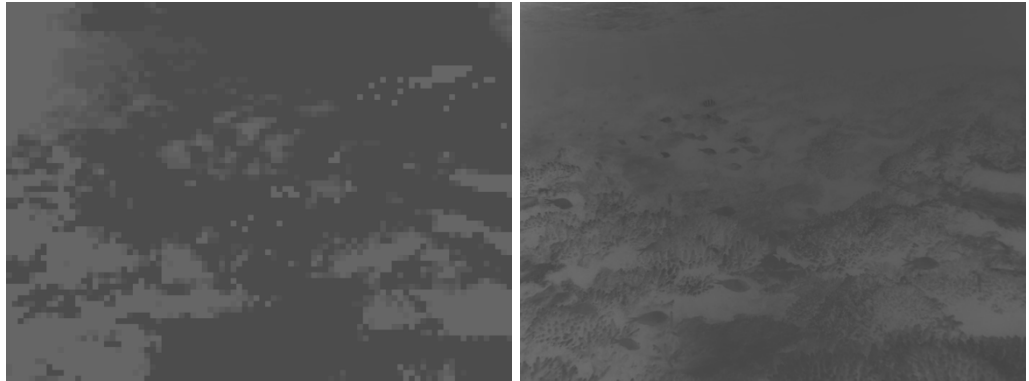


Figure 3.6, Transmission map refinement via image guided filtering, left: coarse transmission map, right: refined transmission map

3.2.2.3 Transmission Map Enhancement

After refinement, the transmission is relatively smoothed. In order to obtain a more accurate transmission map and extract more details from it, the refined transmission map should further be enhanced to improve its texture and details. Since an image can be separated into two parts, one is smooth component, another is detailed component, the transmission map also can be rewritten as this type.

$$t = t_{smooth} + t_{detail} \quad (3-17)$$

where t_{smooth} is the smooth component of transmission map while t_{detail} is the detailed component. For smooth component, we can derive it by using a blur filter. Gaussian low-pass filter (GLPF) is an effective smoothing filter, the idea of Gaussian blur is computing the mean value of center pixel and its surround pixels by utilizing a convolution kernel, and larger the kernel is, smoother the image is. The Gaussian convolution kernel can be represented as:

$$G(x, y) = \frac{1}{2\pi\sigma^2} \cdot e^{-\frac{(x^2+y^2)}{2\sigma^2}} \quad (3-18)$$

where σ is the scale parameter of Gaussian blur. Therefore, the smooth component can be obtained by smoothing the refined transmission map with Gaussian low-pass filter.

$$t_{smooth} = t * G \quad (3-19)$$

Then the detailed component can be derived as the difference between t and t_{smooth} .

$$t_{detail} = t - t_{smooth} \quad (3-20)$$

After that, the enhanced transmission map is calculated by:

$$t_{enhanced} = t_{smooth} + \alpha \cdot t_{detail} \quad (3-21)$$

where α is the enhancement parameter to control the amplified degree of detailed component.



Figure 3.7, Enhanced transmission map, left: refined transmission map, right:
enhanced transmission map

After enhancement, we are able to obtain a well mapped transmission map, which can express the depth information well, in order to show the result of transmission map refinement and enhancement, we introduce the standard deviation and average gradient as the assessment criteria to evaluate the performance of each transmission map, where standard deviation (STD) reflects the high frequency components of image and the higher standard deviation (STD) is, the higher image contrast is, while average gradient reflects the velocity of the changes of minor details in the image, it can represent the features of texture transform and the degree of clearness well.

$$\sigma^2 = \frac{1}{M \cdot N} \cdot \sum_{x=1}^M \sum_{y=1}^N \{I(x, y) - Mean\}^2 \quad (3-22)$$

$$\bar{g} = \frac{1}{M \cdot N} \cdot \sum_{x=1}^M \sum_{y=1}^N \sqrt{\frac{[I(x, y) - I(x+1, y)]^2 + [I(x, y) - I(x, y+1)]^2}{2}} \quad (3-23)$$

Where σ^2 is the standard deviation of image, *Mean* is the average pixel value of image, \bar{g} represents the average gradient and $M \cdot N$ stands for the number of pixels in the image, and each of them represents the size of image.

Table 3.1, Comparison of three transmission maps

	<i>Coarse trans.</i>	<i>Refined trans.</i>	<i>Enhanced trans.</i>
Standard Deviation	10.45	12.56	15.03
Average Gradient	0.51	1.22	2.06



Figure 3.8, Comparison of three transmission maps

It is obvious to see that the standard deviation and average gradient are well improved after refinement and enhancement. The enhancement transmission map shows abundant information of details and texture, which is further utilized to generate the transmission of each color component.

3.2.2.4 Enhanced Transmission Map for Each Color Component

As mentioned before, the transmission maps are various among different color components due to different light absorption abilities for light beams with different wavelength. After obtaining the enhanced transmission map, each color component's transmission map can be derived by exploring the intrinsic relationship and difference among color components. Since underwater images always dominated by one color, i.e., greenish or bluish, and other color components are attenuated, the average pixel value of each color component, although not very accurate, can reflect the attenuation ratio of each color component in water. And it is known that the vertical depth of a given underwater image is hard to estimate due to insufficient prior knowledge and information provided by the image, so the average pixel value can further be utilized to estimate the transmission map for each color component.



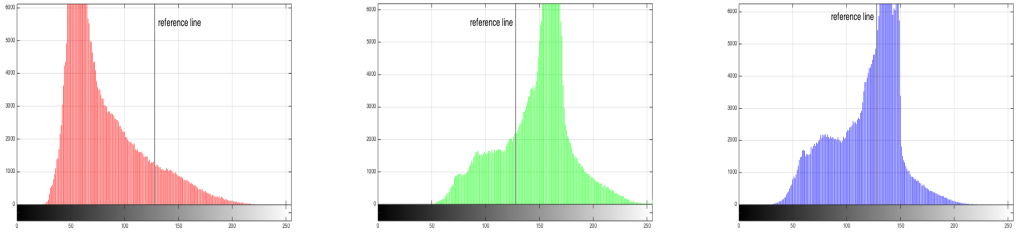


Figure 3.9, Display of each color channel, left to right: red channel and its histogram, green channel and its histogram, blue channel and its histogram

Using a reference line, we can derive the intensity of each color component in Figure 3.9. As mentioned before, underwater images often show bluish or greenish, the average intensity of the image in Figure 3.9, green channel is highest, following by blue channel and red channel is lowest. We are able to get the intrinsic information that the average pixel intensities also contain the attenuation coefficient of each color component.

In the underwater optical model, the formation of transmission map can be simplified as $t(x) = e^{-c \cdot d(x)}$, where c is the total attenuation coefficient and $d(x)$ is the distance from camera to the objects. Due to different light absorption abilities of water for different wavelength light beams, the total attenuation coefficients of different color components are diverse. Meanwhile, the average pixel value generally reflects the relative attenuation ratio of each color component, and the lower value of transmission map is, the higher contrast of restored image is. We firstly define the enhanced transmission map is transmission map of the color component with highest average pixel value. In order to define simply, we suppose that blue component has the highest average pixel value.

$$t_b(x) = t_{enhance}(x) = e^{-c_b \cdot d(x)} \quad (3-24)$$

At the same time, the transmission map of other color components can be written as,

$$t_r(x) = e^{-c_r \cdot d(x)}, t_g(x) = e^{-c_g \cdot d(x)} \quad (3-25)$$

then using $t_b(x)$ to express $t_r(x)$ and $t_g(x)$,

$$t_r(x) = (t_b(x))^{\frac{c_r}{c_b}} = (t_b(x))^{\beta_r}, t_g(x) = (t_b(x))^{\frac{c_g}{c_b}} = (t_b(x))^{\beta_g} \quad (3-26)$$

where β_r and β_g are the relative attenuation ratios and can be estimated by average

pixel value. To simplify the computation, we define that $\beta_r = \text{mean}(I_b)/\text{mean}(I_r)$, $\beta_g = \text{mean}(I_b)/\text{mean}(I_g)$.



Figure 3.10, The transmission map of each color component, from left to right: red channel, green channel and blue channel

3.2.3 Dehazing and Color Correction

After estimating the background light and transmission map of each color component, we can restore the underwater image via simplified physical model formation,

$$J_\lambda^T(x) = \frac{1}{t_\lambda(x)} \cdot (I_\lambda(x) - A(\lambda)) + A(\lambda) \quad (3-27)$$

where $\lambda \in \{r, g, b\}$, and $J_\lambda^T(x)$ is the restoration image. However, the result of formation above can not guarantee the intensities of restored image lie in the display area $[0,1]$ or $[0, 255]$, so a simple minimum-maximum normalization of intensity values is utilized to map them to the display interval. Meanwhile, although normalization method shows some effect on color correction, $J_\lambda^T(x)$ still suffers from part of light attenuation in the vertical direction and cause color distortion. Thus, color correction method should be introduced to solve this problem. For this case, a white balance method is used to execute the vertical direction compensation to obtain the final enhanced illuminance component $J_\lambda(x)$, which can achieve good results.

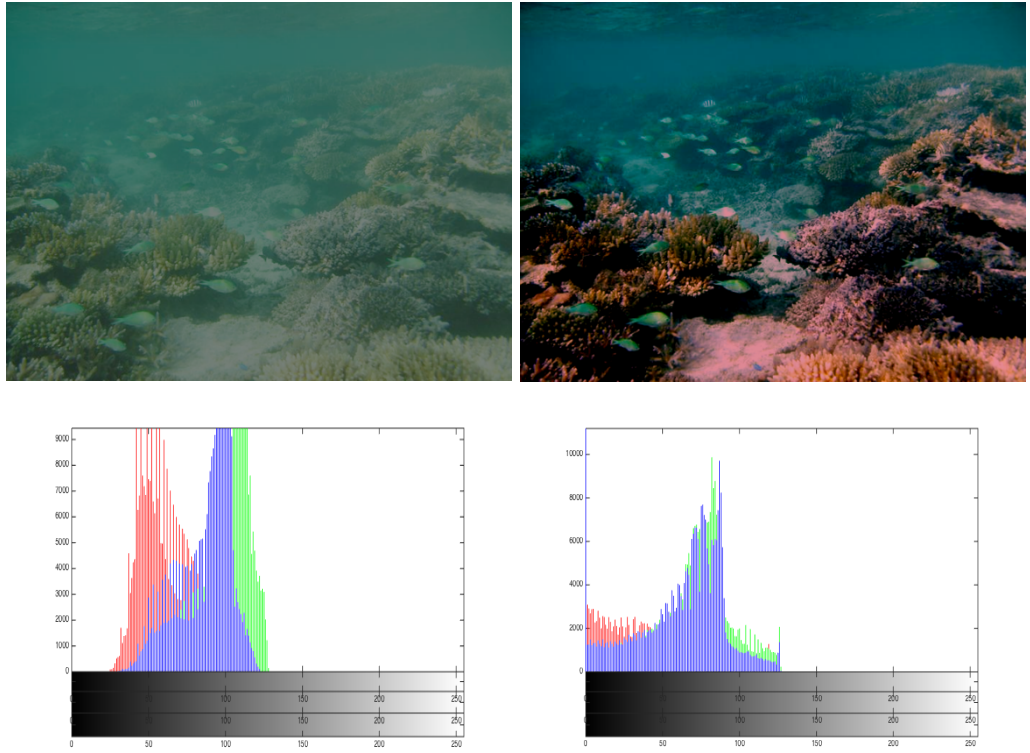


Figure 3.11, The processed result of illuminance component, left: input image and its histogram, right: output image and its histogram

3.3 Color Correction for Reflectance Component

The reflectance component reflects the texture and details of underwater scenes, and we have mentioned that it is considered to be free of backscatter. Thus, the reflectance component only suffers from color distortion caused by energy absorption of water. In order to deal with this issue, the color correction method should be introduced. Color constancy based color correction methods are excellent way to handle this process, which shows great balance between the correction performance and information loss, since the general procedures of such methods include darkest and brightest pixels' truncation and histogram stretch, which may cause some undesired phenomena of texture information loss.

By comparison, the simplest color balance (SCB) method is a better method for this case. The algorithm is fast and efficient, since it only simply stretches the pixel

values of the three color channels while preserves the information of image as much as possible by manually setting different truncation ratio of different color channel, so that their histograms are able to occupy the maximal display range [0,255] (or [0,1]). In order to execute fast stretch process, an affine transform function $ax + b$ is applied on each color channel to map pixel values from minimum 0 to maximum 255 (or 1) by computing proper a and b . However, few aberrant pixels of many images already map the maximum and minimum values, so truncation is used to improve color performance by “clipping” a small percentage of pixels with highest values and lowest values before applying affine transform function. Actually, this process will cause more or less white and black regions in images, which may look unnatural. Thus, the number of truncated pixels must be as less as possible. In general, although this algorithm is not real white balance algorithm since it does not focus on correcting the color distributions, it can provide white balance effect and contrast enhancement to some degree.

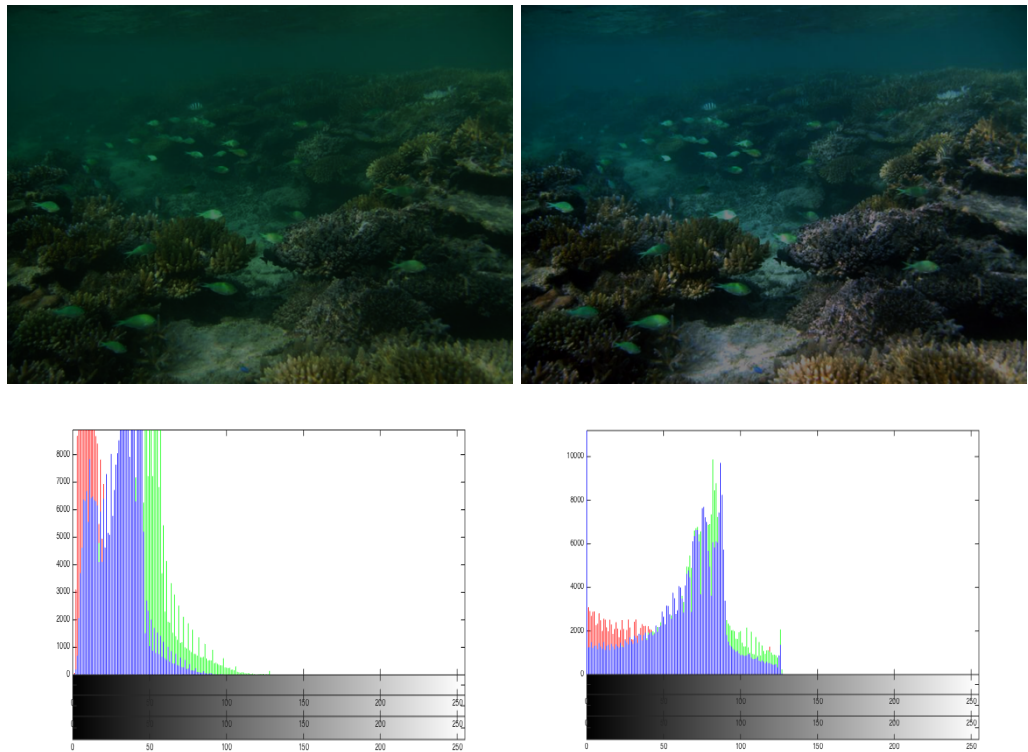


Figure 3.12, The processed result of reflectance component, left: input image and its histogram, right: output image and its histogram

3.4 Fusion Process

3.4.1 Weights of the Fusion Process

After deriving the enhanced illuminance and reflectance components, a fusion-based method is introduced to combine these two images and generate the final free backscatter and color distortion image. For fusion techniques, one of the crucial steps is computing the weight maps of input images. In order to represent different features of input images well, we use several weight map methods to measure the features of input images and then combine them together to derive the normalized weighted maps. In practice, we choose three weight maps, luminance weight map, saliency weight map and exposedness weight map.

Luminance weight map [15], W_L , which represents the luminance parameter of each image component. This weight map is generated by calculating STD between r , g and b color channels and the luminance value l , where the luminance value l is derived by:

$$l = \alpha \cdot r + \beta \cdot g + \gamma \cdot b \quad (3-28)$$

where $\alpha + \beta + \gamma = 1$, each represents the weight parameter of each color component, and normally we set $\alpha = 0.299$, $\beta = 0.587$ and $\gamma = 0.114$. It generates high values correlated with the preservation degree of each input region, while the multi-scale blending ensures a seamless transition between the inputs [15]. However, this weight map is able to correctly reflect the luminance degree of image and show greater enhancement for degraded image, it shows negative effects on contrast and colorfulness. In order to compensate the drawbacks, following weight maps are introduced.

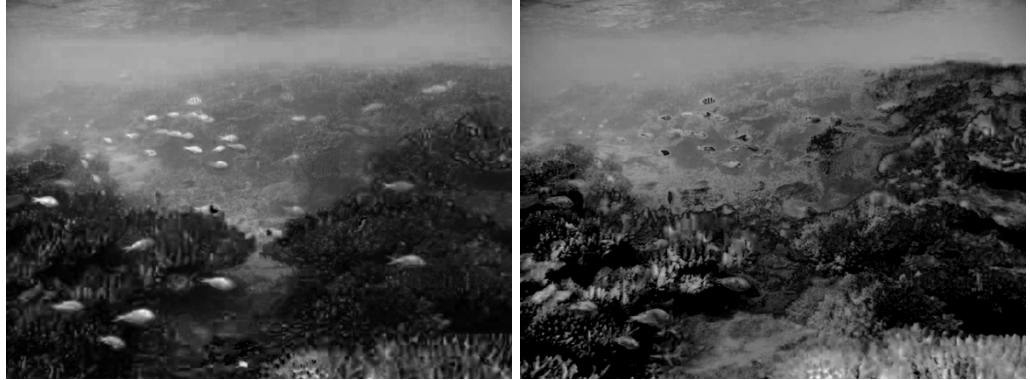


Figure 3.13, Luminance weight maps of two image components, left: reflectance component, right: illuminance component

Saliency weight map [16], W_S , which reflects the salient objects and points in an image, and it aims to emphasize these discriminating objects of underwater scenes. In order to obtain the saliency map, the algorithm of Achanta et al. [25] based on biological concept of center-surround contrast is applied due to its computationally efficient and time saving. One of the drawbacks of applying saliency map is overestimation of highlighted areas, thus exposedness weight map is utilized to guarantee the accuracy and protect the mid tones of image.



Figure 3.14, Saliency weight maps of two image components, left: reflectance component, right: illuminance component

Exposedness weight map [16], W_E , which evaluates the status of exposed pixels. It provides an operator to protect local contrast to be non-exaggerated or non-understated. Generally, pixel values close to mean value is likely to have higher exposed appearance. The map is written as Gaussian-modeled distance to the mean

value:

$$W_E = e^{-\frac{(I(x)-\bar{I})^2}{2\cdot\sigma^2}} \quad (3-29)$$

where σ is the standard deviation, $I(x)$ denotes pixel value located at position x and \bar{I} represents mean value. From the formation, pixels close to mean value have higher weight while pixels with larger distances are associated with over-exposed and under-exposed regions. Consequently, these three weight maps are able to produce well preserved appearance of fused images.

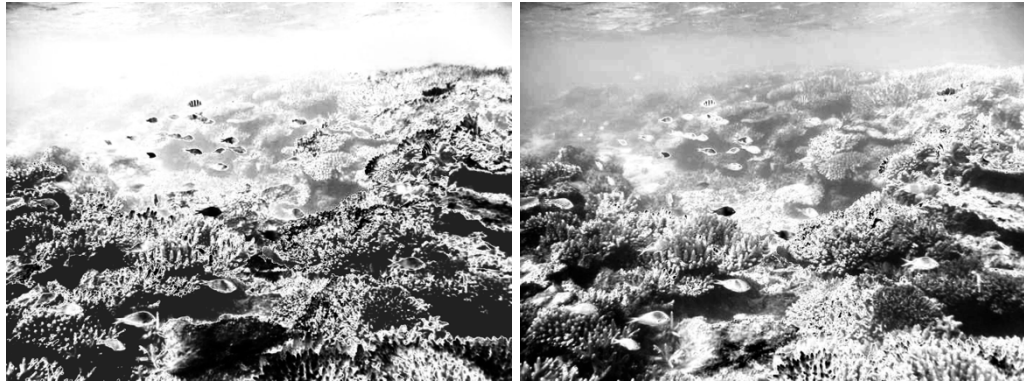


Figure 3.15, Exposedness weight maps of two image components, left: reflectance component, right: illuminance component

3.4.2 Multi-scale Fusion Process

In general, these three weight maps are complementary and able to express the features of input images well. To yield the normalized weight map from these three featured weight maps, we can simply compute as:

$$W_{norm} = \sum_{k=1}^K W_k \quad (3-30)$$

where W_k is the k^{th} weight map.

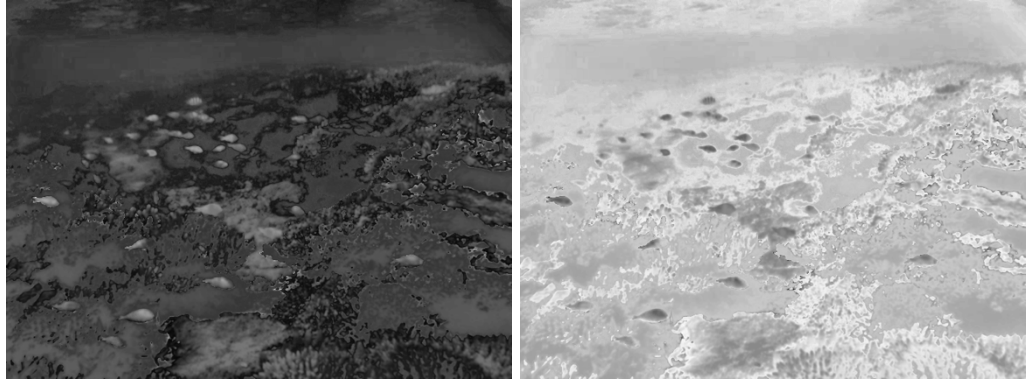


Figure 3.16, Normalized weight maps of two image components, left: reflectance component, right: illuminance component

And further the final free backscatter and color distortion image can be derived as:

$$\mathcal{R}_\lambda = \sum_{n=1}^N W_{norm}^n \cdot J_\lambda^n \quad (3-31)$$

where \mathcal{R}_λ is the λ color component of final output image, J_λ^n is the λ color component of n^{th} input image.



Figure 3.17, The final output image via naive fusion process

However, we can derive from Figure 3-17, the naive approach to directly fuse the inputs and the weight maps introduces undesirable halos. Thus, in order to improve the performance, we practically utilize a multi-scale Gaussian and Laplacian pyramid decomposition technology to execute fusion process. In this method, each input is decomposed to several layers with different scales by Laplacian operator and Gaussian kernel. Meanwhile, higher layers are generated by differentiating the original image and filtered image of lower layer in Gaussian pyramid. Thus, the Laplacian pyramid is a set of quasi-bandpass versions of image [16].

At the same time, the Gaussian pyramid of normalized weight map W_{norm} is calculated, so that both Laplacian and Gaussian pyramids have same levels, and fusion process can be written as:

$$\mathcal{R}_\lambda^l = \sum_{n=1}^N G^l\{W_{norm}^n\} \cdot L^l\{J_\lambda^n\} \quad (3-32)$$

where $L^l\{J_\lambda^n\}$ is Laplacian pyramid of the λ color component of n^{th} input image, $G^l\{W_{norm}^n\}$ is n^{th} normalized weight map and l is pyramid levels. Since Laplacian multi-scale strategy performs relatively fast and balances a good trade-off between speed and accuracy, the restored output image can achieve excellent result.



Figure 3.18, The final output image via multi-scale Gaussian and Laplacian fusion process

Chapter 4

Comparison, Evaluation and Analysis

In this chapter, the proposed underwater objects visibility enhancement method is compared to some state-of-art methods, which are evaluated by the images collected from representational underwater test images and different metrics are utilized to compare the restoration performances of these methods.

4.1 Measurements of Underwater Imaging Performance

4.1.1 Basic Evaluation Index for Underwater Imaging Performance

Expect for the subjective assessment, this subsection introduces several basic underwater image quality metrics to evaluate and analyze the performance of different underwater imaging methods, including gray average, standard deviation, average gradient, RGB color space mapping and etc.

The mean value and standard deviation are the basic and wide evaluations to measure the quality of images, which are able to reflect the intensity and contrast information of images well. Generally, gray average value of an image reflects the integral intensity, and higher the gray average is, higher the intensity is, while standard deviation of an image reflects the high frequency component of an image, which is related to the image contrast, higher the standard deviation is, higher the contrast is as well as greater color information. Meanwhile, Jobson et al. [26] indicate that an image shows good integral quality performance when its gray average between 100 and 200 and its standard deviation between 35 and 80 after they analyzed and statistic a large amount of images,

$$Mean = \frac{1}{M \cdot N} \cdot \sum_{i=1}^M \sum_{j=1}^N I(i, j) \quad (4-1)$$

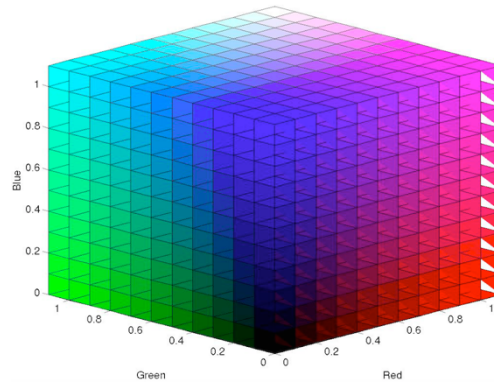
$$\sigma^2 = \frac{1}{M \cdot N} \cdot \sum_{x=1}^M \sum_{y=1}^N \{I(x, y) - Mean\}^2 \quad (4-2)$$

where *Mean* is the gray average value of the image and σ^2 is the corresponding standard deviation. However, the average gradient reflects the velocity of the changes of minor details in the image, it can represent the features of texture transform and the degree of clearness well, and its definition is,

$$\bar{g} = \frac{1}{M \cdot N} \cdot \sum_{x=1}^M \sum_{y=1}^N \sqrt{\frac{[I(x, y) - I(x+1, y)]^2 + [I(x, y) - I(x, y+1)]^2}{2}} \quad (4-3)$$

\bar{g} represents the average gradient and $M \cdot N$ stands for the number of pixels in the image, and each of them represents the size of image.

Besides, three dimensional RGB color space is able to represent all the 8-bits color within its cubic space. As shown in the Figure 4.1, each coordinate axis represents a color, i.e., red, green and blue, while it also includes the intensity of the pixels. In the RGB color space, an image with good dynamic compression range is more likely to map as much space as possible. For distorted images such as low illumination image or color casting image, their mapping results are gathered in some corners of RGB color space. For instance, the underwater image who suffers from heavy color casting and shows greenish, its mapping result is gathered in the left corner in the color space. Thus, RGB color space is utilized to analyze the integral dynamic compression range.



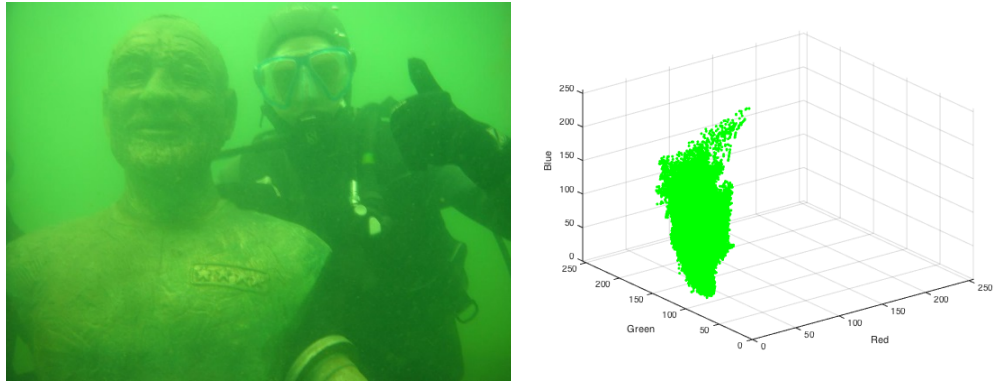


Figure 4.1, RGB color space model and an example of image mapping in the space

Since underwater imaging often plays a role of pre-processing for the certain image processing such as image decomposition, pattern recognition, visual tracking and so forth. The restored scenes and objects in the image or video needs to have a clear texture and details. Thus, we introduce the Sobel operator to detect the edges of restored images and calculate the score of the edges, where Sobel operator is shown below:

$$X_{direction} = \begin{bmatrix} 1 & 2 & 1 \\ 0 & 0 & 0 \\ -1 & -2 & -1 \end{bmatrix}, \quad Y_{direction} = \begin{bmatrix} 1 & 0 & -1 \\ 2 & 0 & -2 \\ 1 & 0 & -1 \end{bmatrix} \quad (4.4)$$

where $X_{direction}$ is used to detect the edges in the vertical direction and $Y_{direction}$ is used to detect the edges in the horizontal direction.



Figure 4-2, an example of edges detection of restored image

However, these basic measurements can not give a comprehensive evaluation of underwater imaging performance, since underwater image suffers various degradations and each of them has their own features, the measurements mentioned above can not cover the whole parts. In general, underwater scenes and objects suffer from color fading, sharpness attenuation and contrast degradation, thus, in order to

evaluate the performance of underwater imaging well, we also need to compare these parts of restored images. So we introduce the underwater image quality metrics measurement to bring a comprehensive evaluation, which will be discussed in the next subsection.

4.1.2 Underwater Image Quality Metrics

In this subsection, we introduce an efficient underwater image quality measurement, UIQM, which is composed of three independent measurements, underwater image colorfulness measure (UICM), underwater image sharpness measure (UISM), underwater image contrast measure (UIConM) [27].

(1) Underwater Image Colorfulness Measure

Most of underwater images are degraded by color casting, and growth with depth increases, while different colors show various attenuating ratio. Generally, red component is disappeared firstly because of the shortest wavelength, while blue and green components attenuate slowly, so underwater scenes are often demonstrated to be bluish or greenish. Moreover, limited lighting conditions also causes severe color desaturation in underwater images. In order to measure the performance of color correction performance, the UICM is utilized to evaluate the performance of underwater image enhancement algorithms, and the Red-Green (RG) and Yellow-Blue (YB) color components are used:

$$RG = R - G \quad (4-5)$$

$$YB = \frac{R+G}{2} - B \quad (4-6)$$

Considering that underwater image often suffers heavy noise, instead of regular statistical values, the asymmetric alpha-trimmed statistical values [28] are used for measuring underwater image colorfulness,

$$\mu_{RG} = \frac{1}{N-T_L-T_R} \sum_{x=T_L}^{N-T_R} \text{Intensity}_{RG}(x) \quad (4-7)$$

where N is the total number of pixels in the RG component and all pixels of the image are sorted such that $x_1 < x_2 < \dots < x_N$, $T_L = \alpha_L \cdot N$ and $T_R = \alpha_R \cdot N$ are the number of smallest and greatest pixel values to be truncated or discarded from the

sorted sequence $x_1 < x_2 < \dots < x_N$. The first-order statistic mean value μ_{RG} represents chrominance intensity, and the average value that is closer to zero in the RG-YB opponent color component implies a better white balance, which means none of the colors are dominant. Further, the second-order statistic variance is defined by:

$$\sigma_{RG}^2 = \frac{1}{N} \cdot \sum_{x=1}^N (Intensity_{RG}(x) - \mu_{RG})^2 \quad (4-8)$$

σ_{RG}^2 represents the pixel activity and a greater variance corresponds to a higher dynamic range. What's more, the first and second order statistic information μ_{YB} and σ_{YB}^2 of the yellow-blue component can be computing in the similar way.

The overall colorfulness coefficient metric which is used for measuring underwater image colorfulness is able to demonstrated in

$$UICM = -0.0268 \cdot \sqrt[2]{\mu_{RG}^2 + \mu_{YB}^2} + 0.1586 \cdot \sqrt[2]{\sigma_{RG}^2 + \sigma_{YB}^2} \quad (4-9)$$

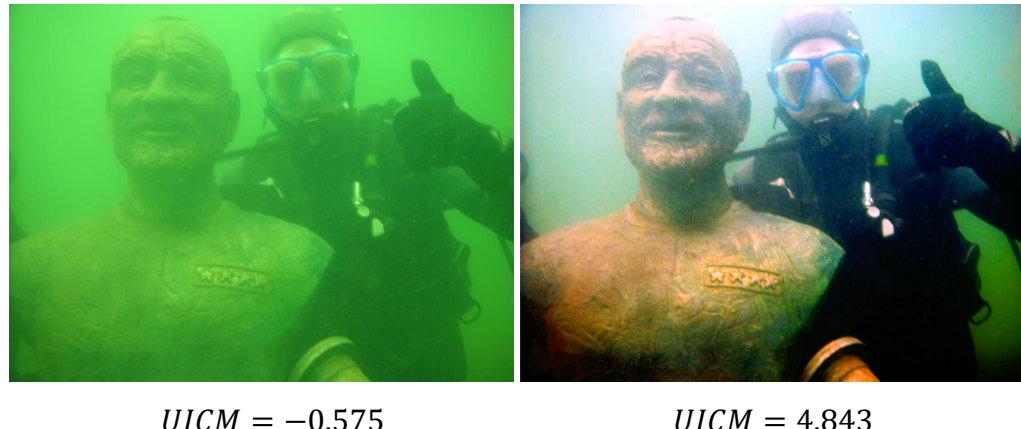


Figure 4.3, UICM example of original image and restored image

Table 4.1, statistic values of UICM for diver image

	μ_{RG}	μ_{YB}	σ_{RG}	σ_{YB}	$UICM$
LEFT	-1.067	61.696	13.194	11.045	-0.575
RIGHT	-1.432	5.03	21.560	25.770	4.843

As shown in the Figure 4-3 and Table 4-1, the $UICM$ of restored image is much greater than original image.

(2) Underwater Image Sharpness Measure

Sharpness reflects the details and edges of an image, and fine captured images are likely to show better sharpness. However, for images captured under the water, severe blurring and distortion occur due to backscatter and absorption. In order to measure the sharpness, the Sobel operator is first applied on each color component to generate the edge maps. Then the obtained edge maps are multiplied to original color component to calculate the gray-scale edge maps. By doing this more efficient, the enhancement measure estimation (EME) measure [27] is utilized to measure the sharpness

$$EME = \frac{2}{m \cdot n} \cdot \sum_{k=1}^m \sum_{l=1}^n \log \left(\frac{I_{max,k,l}}{I_{min,k,l}} \right) \quad (4-10)$$

where the image is divided into $m \cdot n$ blocks, and obtain the maximal and minimal pixel values in each block, $I_{max,k,l}/I_{min,k,l}$ indicates the relative contrast ratio within each block. Then the underwater image sharpness measure (UISM) can be written as:

$$UISM = \sum_{c=1}^3 \lambda_c \cdot EME(\text{grayscale edge}_c) \quad (4-11)$$

where λ_c is the weight coefficient of each color component, normally, $\lambda_R = 0.299$, $\lambda_G = 0.587$, $\lambda_B = 0.114$ for red, green and blue color channels.

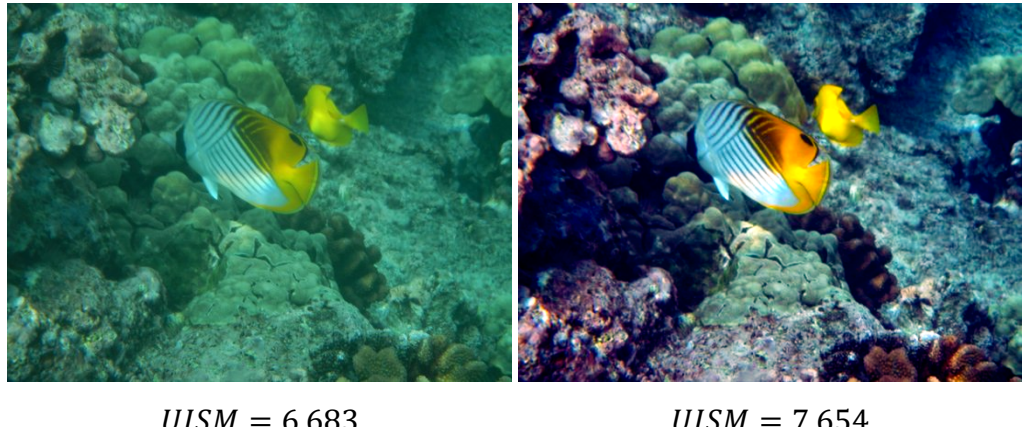


Figure 4.4, UISM example of original image and restored image. Left: underwater backscatter image, right: descattered image by proposed method, it seems that original image suffers heavier blurring effect.

(3) Underwater Image Contrast Measure

Contrast is the attribute related to underwater visual performance. For underwater

images, contrast degradation is usually caused by backscattering. The contrast performance can be measured by the logAMEE measurement, and it is defined by:

$$\log AMEE = \frac{1}{m \cdot n} \cdot \sum_{k=1}^m \sum_{l=1}^n \frac{I_{max,k,l} - I_{min,k,l}}{I_{max,k,l} + I_{min,k,l}} \cdot \log \left(\frac{I_{max,k,l} - I_{min,k,l}}{I_{max,k,l} + I_{min,k,l}} \right) \quad (4-12)$$

and the underwater image contrast measure can be written as:

$$UIConM = \log AMEE(Intensity) \quad (4-13)$$



Figure 4.5, UIConM example of original image and restored image. Left: original underwater image, right: contrast enhanced image by proposed method, which shows greater improvement of contrast.

(4) Underwater Image Quality Measure

It has been demonstrated that underwater images can be modeled as linear superposition of absorbed and scattered components [27]. Meanwhile, the water absorption and backscatter by dusk-like particles are able to cause color casting, sharpness attenuation and contrast degradation. Therefore, it is reasonable to use the linear model for generating the overall underwater image quality measure, thus the underwater image quality measure (UIQM) is given by:

$$UIQM = \alpha \cdot UICM + \beta \cdot UISM + \gamma \cdot UIConM \quad (4-14)$$

where the colorfulness, sharpness and contrast measure are combined together through the linear function designed above, and α , β , and γ are the weight coefficients to control the importance of each measure and balance their values. Generally, these parameters are set to be $\alpha = 0.0282$, $\beta = 0.2953$ and $\gamma = 3.5753$.

4.2 Experiment Results and Evaluations

In this subsection, we use the measurements mentioned above to evaluate the performance of proposed underwater objects visibility enhancing method as well as comparison to the state-of-art methods. For this case, we compare the performance of our method to several state-of-art methods in recent years, where most of them also achieves excellent performance for the underwater imaging issue. Generally, we introduce the methods proposed by Ancuti et al. [16], Galdran et al. [5], Fu et al. [17], He et al. [4], Getreuer et al. [11] and etc.

4.2.1 Basic Evaluation Measurements among Different Methods

Images captured in the different underwater environments often show various attenuation and degradation degree, which causes that an underwater imaging method may performs well for several certain underwater environment conditions, but weak for other conditions. We choose a set of images for evaluation.



Diver Image

Open Scene Image

Fish Image

Figure 4.6, The set of images chosen to evaluation and comparison

We first process (a) image shown in the Figure 4-6 by several state-of-art methods and the result is shown below.

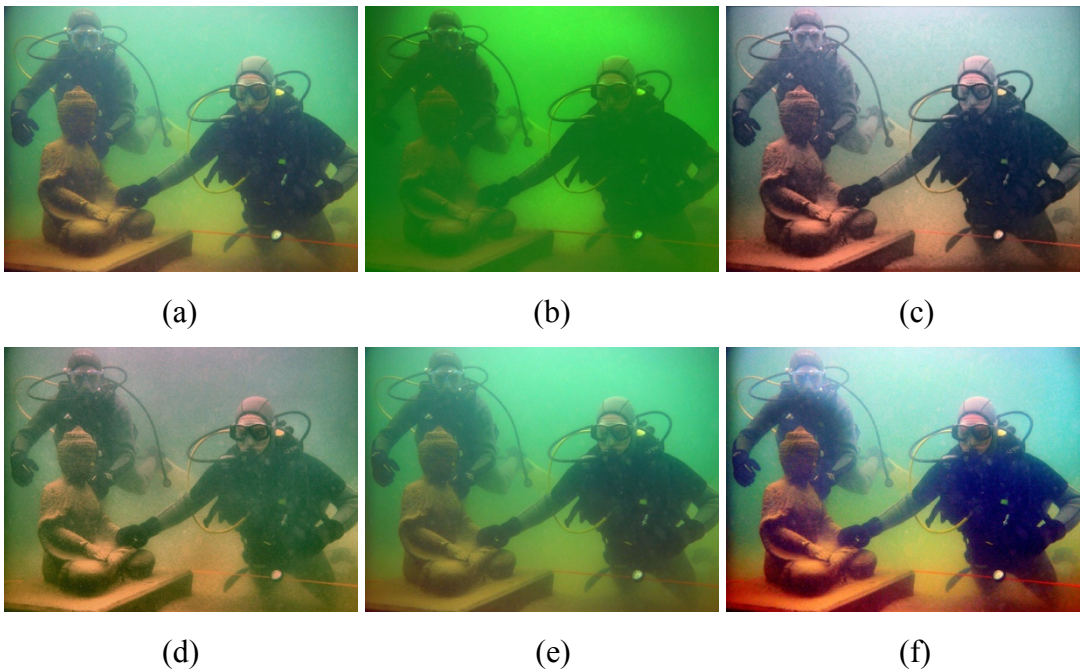


Figure 4.7, Results on the diver image via different methods. (a) ACE. (b) Histogram equalization (HE). (c) Fu et al. (d) Ancuti et al. (e) Galdran et al. (f) Proposed method.

We see that on the diver image, the histogram equalization (HE) method fails to correct and enhance the visibility of degraded image, while ACE method shows good color correction as well as proper contrast enhancement, the restored results generated by other three methods also achieve color correction and contrast enhancement, their mean value, standard deviation and average gradient are greatly improved, as shown in the table 4.1. Expect the highest mean value, standard deviation and average gradient, the objective visual performance of the result obtained by our method are better than other methods.

Table 4.2, Basic visibility recovery coefficient of diver image

	<i>Original</i>	<i>ACE</i>	<i>HE</i>	<i>Fu.</i>	<i>Ancuti.</i>	<i>Galdran.</i>	<i>Proposed.</i>
<i>Mean Value</i>	88.7	117.3	70.3	114.0	103.9	104.2	124.4
<i>Standard Deviation</i>	21.00	45.63	25.94	61.76	38.81	42.87	80.33
<i>Average Gradient</i>	1.31	4.90	1.91	3.93	3.94	2.88	5.89

Moreover, we can see from the RGB color space of the original images and restored results that all the pixels of original image maps into the RGB color space are gathered in the left corner, where is large green value and small blue and red value, and other methods achieve more or less stretch of the pixel mapping results. It is obvious that the mapping result of our method is best and it maps the largest area in the RGB color space, which means it has the best integral dynamic compression range. However, many mapping pixels of our method is mapped onto the boundary, i.e., dark region (pixel value is 0) and brightest region (pixel value is 255), it indicates that there is information loss of our method.

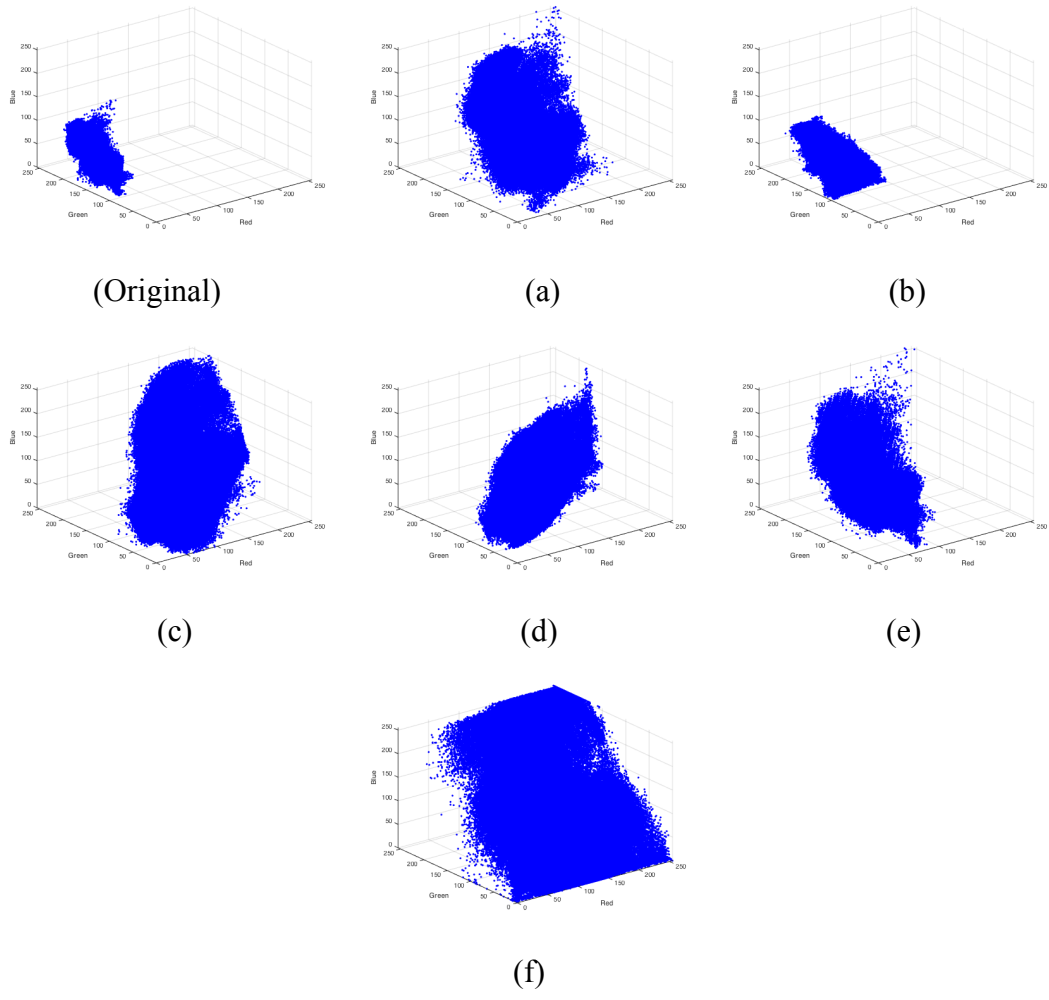


Figure 4.8, RGB color space mapping of different restoration methods on diver image. (a) ACE. (b) Histogram equalization (HE). (c) Fu et al. (d) Ancuti et al. (e) Galdran et al. (f) Proposed method.

As we mentioned before that underwater imaging often plays a role of pre-processing for the certain image processing such as image decomposition, pattern recognition, visual tracking and so forth. The texture and details are important for images and they are also the evaluation standards to measure the performance of an image, so we will compare the edge information of these restored results.

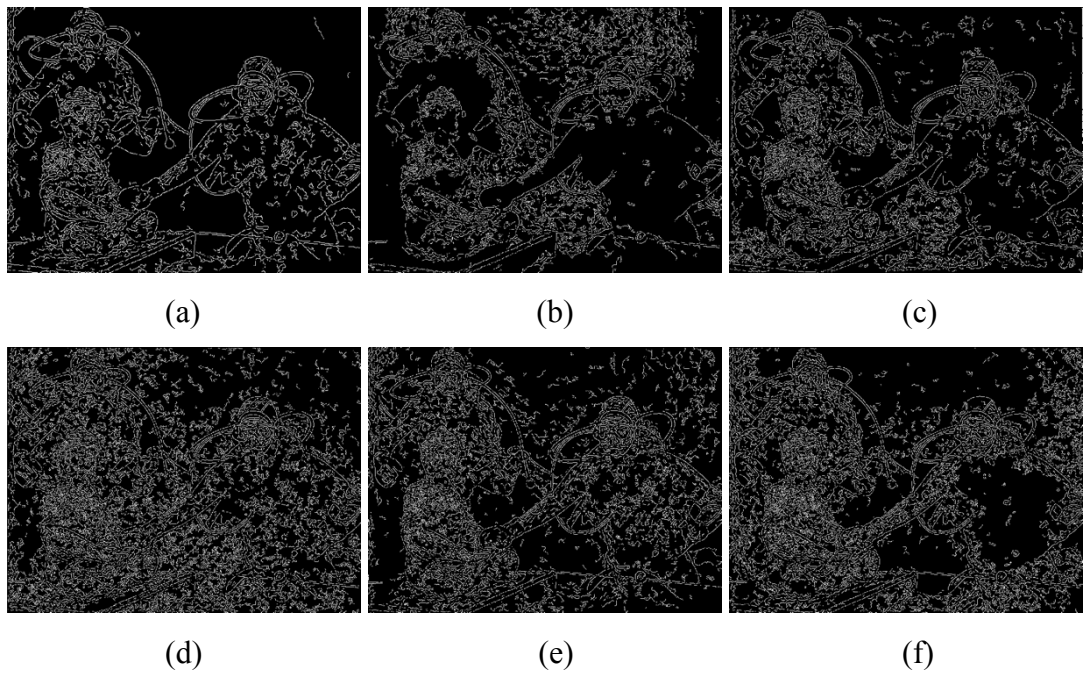


Figure 4.9, Edge information of different restoration methods on diver image. (a) ACE. (b) Histogram equalization (HE). (c) Fu et al. (d) Ancuti et al. (e) Galdran et al. (f) Proposed method.

Figure 4.9 gives the edge information of different restoration results, Ancuti et al. [16] preserves the edges best, following by the Galdran et al. [5]. Due to the information loss effects, the edge of our restoration result does not outperform the two results, but still better than other three methods.

For this diver image, our method achieves the integrally best performance, although it seems that some information loss exists. Actually, our method not only achieves excellent performance for heavy color casting images, like diver image above, but also performs well on images captured in different underwater environments. For the

open scene image, the restoration results are shown below.

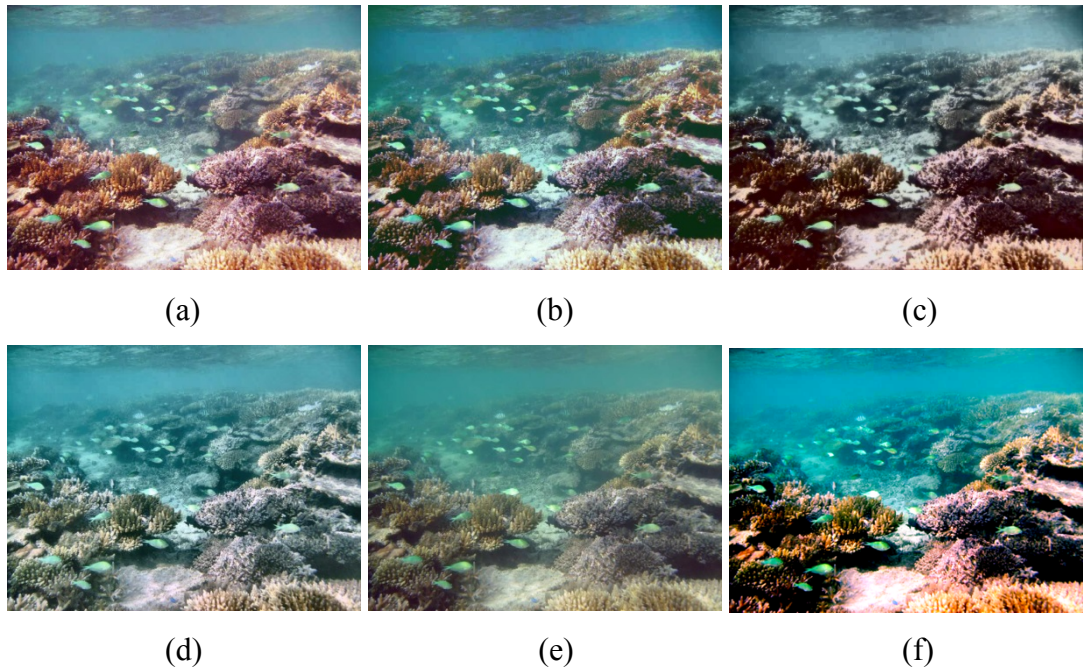
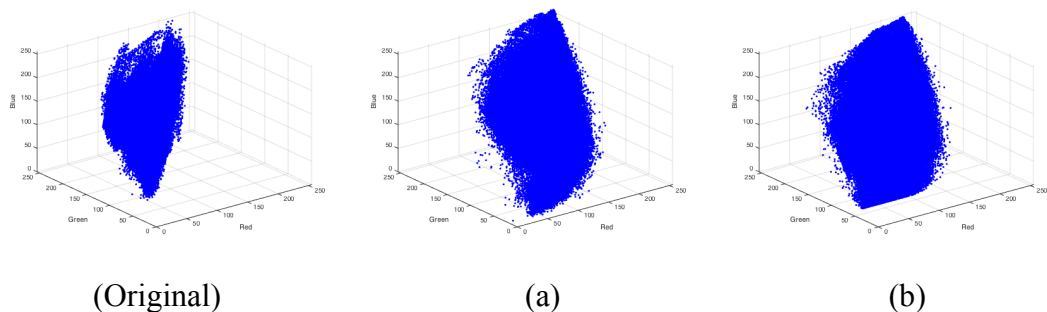


Figure 4.10, Results on the open scene image via different methods. (a) ACE. (b) Histogram equalization (HE). (c) Fu et al. (d) Ancuti et al. (e) Galdran et al. (f) Proposed method.

Table 4.3, Basic visibility recovery coefficient of open scene image

	<i>Original</i>	<i>ACE</i>	<i>HE</i>	<i>Fu.</i>	<i>Ancuti.</i>	<i>Galdran.</i>	<i>Proposed.</i>
<i>Mean Value</i>	116.1	125.2	111.1	101.3	121.1	110.3	108.9
<i>Standard Deviation</i>	32.88	53.48	55.91	62.87	50.32	38.12	76.31
<i>Average Gradient</i>	5.64	10.35	10.70	9.64	11.56	6.65	12.79



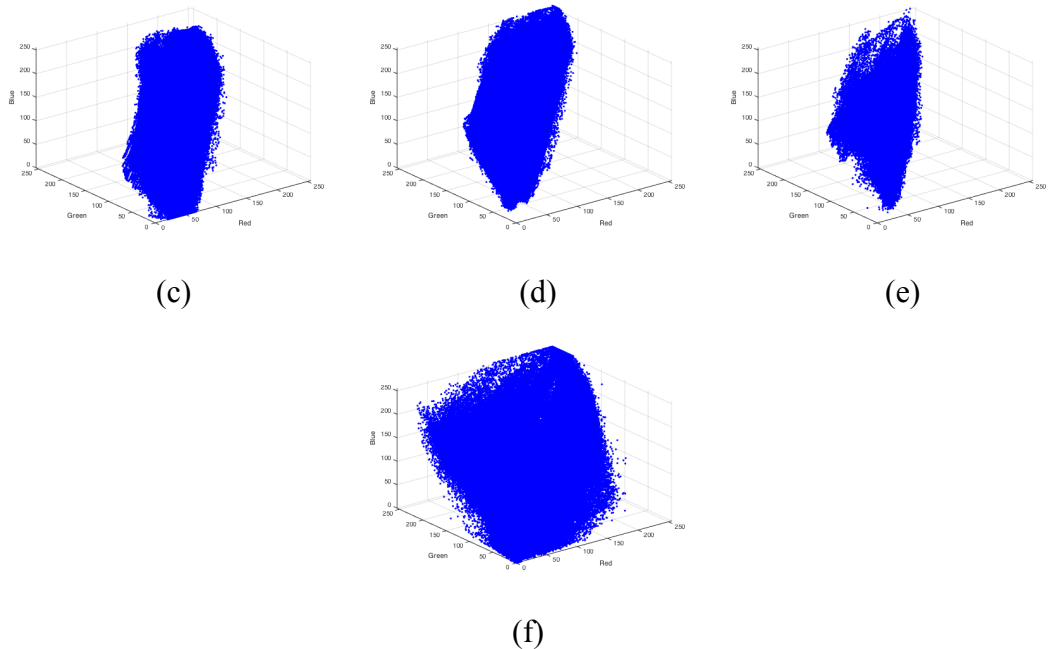


Figure 4.11, RGB color space mapping results on open scene image. (a) ACE. (b) Histogram equalization (HE). (c) Fu et al. (d) Ancuti et al. (e) Galdran et al. (f) Proposed method.

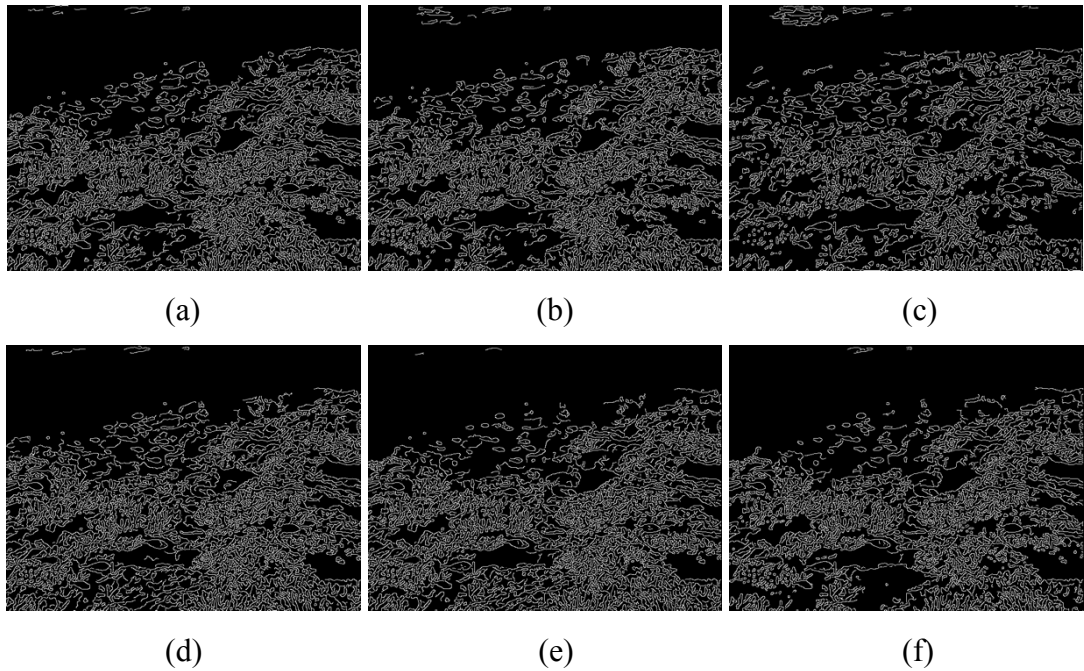


Figure 4.12, Edge information of different restoration methods on open scene image. (a) ACE. (b) Histogram equalization (HE). (c) Fu et al. (d) Ancuti et al. (e) Galdran et al. (f) Proposed method.

Although the ACE method outperforms our method in mean value, our method still performs best among all these methods, which has excellent visual performance as well as good RGB color space mapping and higher contrast degrees, but its edge information does not achieve well because of the information loss. Among these methods, we can see that Fu et al. over-enhancing the distorted image, which causes severe color distortion and noise amplification, thus the integral performance of enhanced image is worse. Galdran et al. solves the effect of color casting and contrast degradation to some degree, but it is not enough, the results still tends to be greenish, while Ancuti et al. gets the good result, not only correcting the color casting but also enhancing the contrast. For histogram equalization method as well as ACE method, which are image processing methods, aim to normalize and regularize the histogram of an image and achieve the contrast enhancement and color correction. By comparison, although the histogram equalization method fails to solve the issue of diver image, it achieves good result for the open scene image, which indicates that this method is not suitable for dense color casting and heavy hazy situation. But for ACE method, it performs well in both of two test images. Moreover, another image enhancement results are shown.

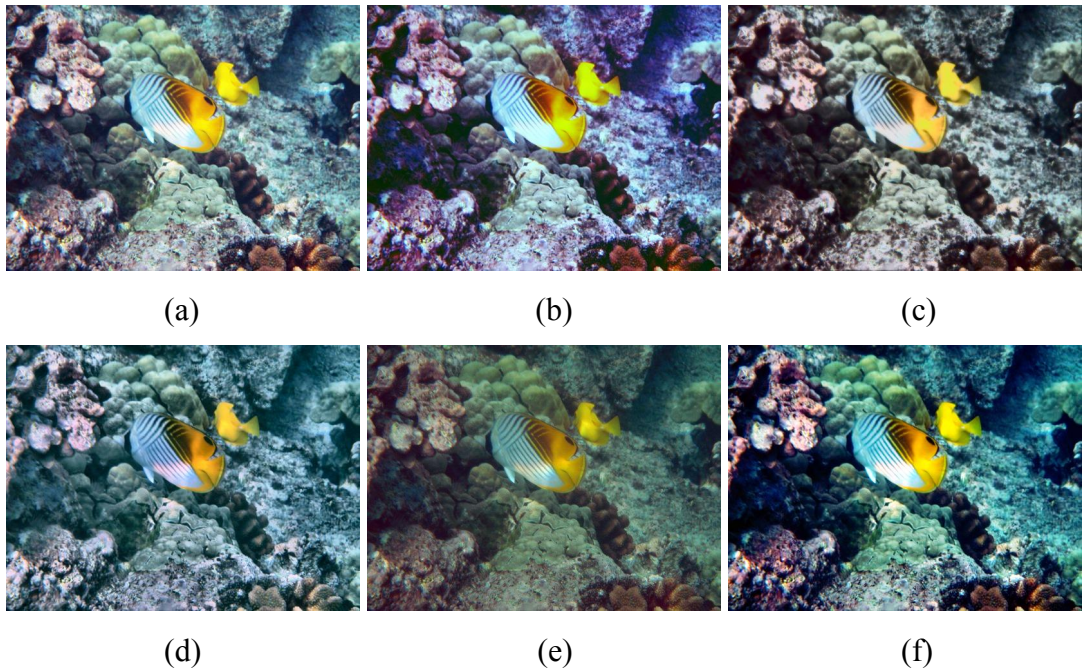


Figure 4.13, Results on the fish image via different methods. (a) ACE. (b) Histogram equalization (HE). (c) Fu et al. (d) Ancuti et al. (e) Galdran et al. (f) Proposed

method.

Table 4.4, Basic visibility recovery coefficient of fish image

	<i>Original</i>	<i>ACE</i>	<i>HE</i>	<i>Fu.</i>	<i>Ancuti.</i>	<i>Galdran.</i>	<i>Proposed.</i>
<i>Mean Value</i>	82.6	118.2	113.2	96.8	107.1	82.6	89.4
<i>Standard Deviation</i>	32.31	59.55	65.51	62.90	57.35	37.46	64.90
<i>Average Gradient</i>	5.86	11.83	12.44	10.46	13.01	6.76	12.29

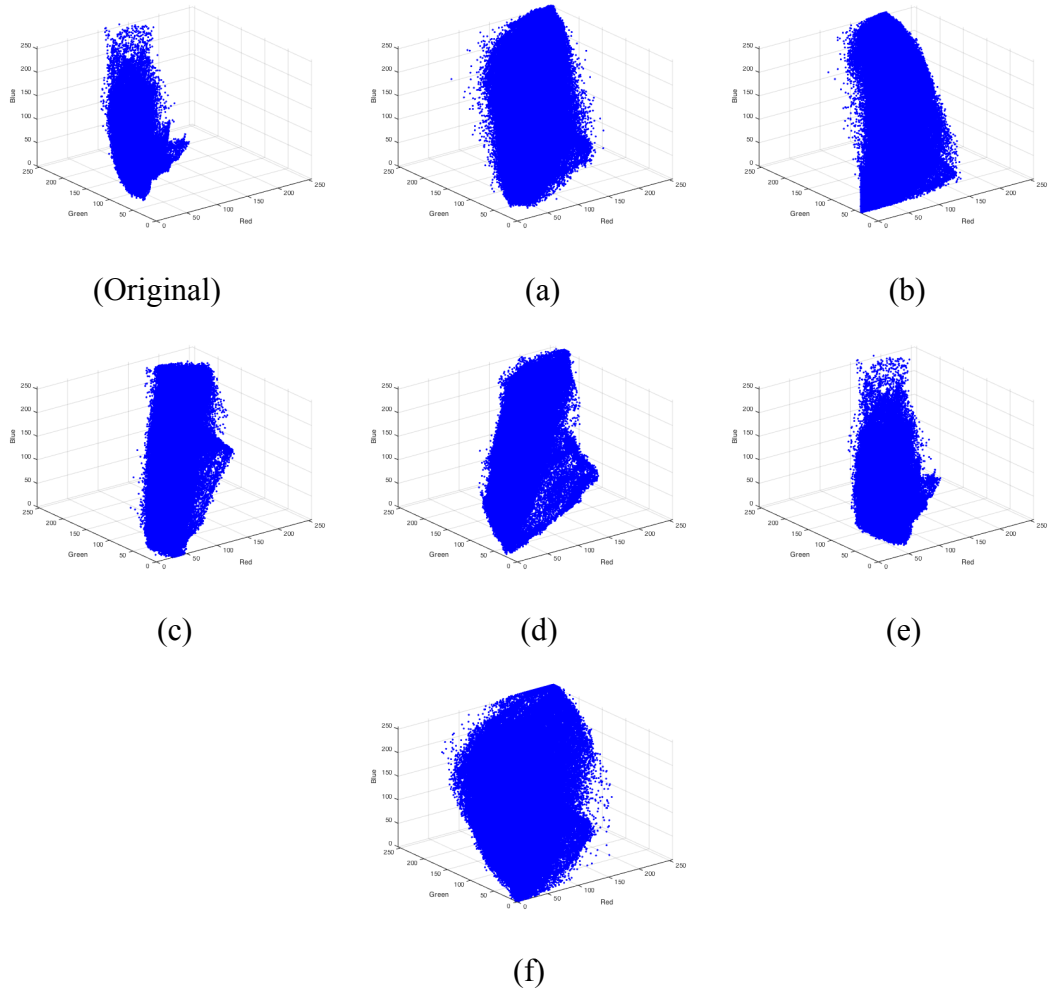


Figure 4.14, RGB color space mapping results on fish image. (a) ACE. (b) Histogram equalization (HE). (c) Fu et al. (d) Ancuti et al. (e) Galdran et al. (f) Proposed method.

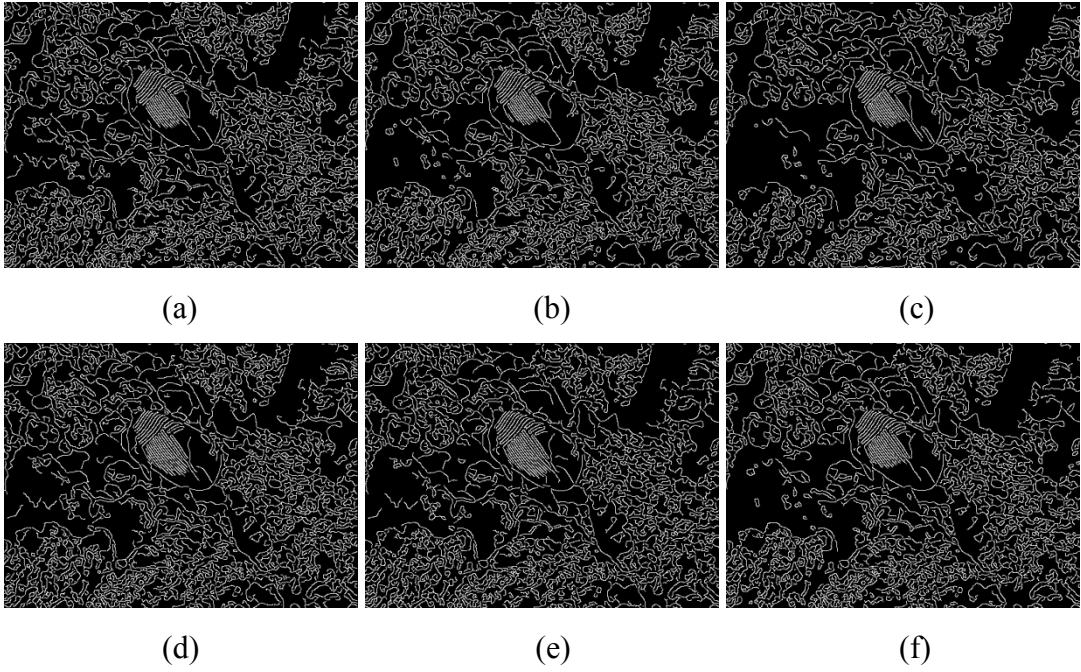
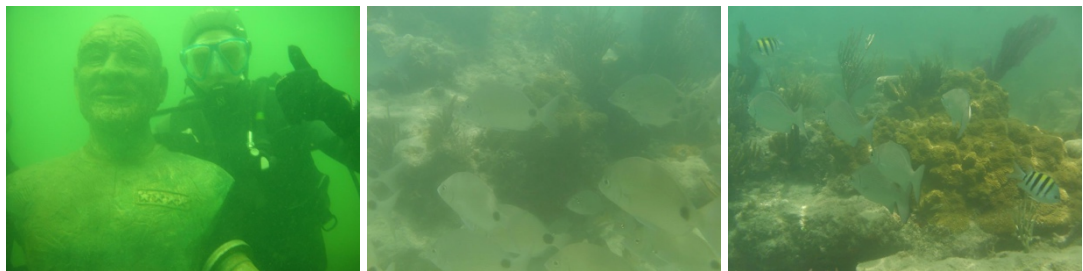


Figure 4.15, Edge information of different restoration methods on fish image. (a) ACE. (b) Histogram equalization (HE). (c) Fu et al. (d) Ancuti et al. (e) Galdran et al. (f) Proposed method.

4.2.2 UIQM Measurement among Different Methods

Although the measurements used in subsection 4.2.1 gives us some performance information of restoration performance of different methods, these measurements are not used to evaluate the underwater imaging issue, so they can only give some certain parts of the comparing results. In order to overcome the drawbacks of traditional image measurements and evaluate the performance of underwater imaging well, we introduce the underwater image quality metrics (UIQM) [27] measurement to give a comprehensive evaluation. Similarly, we also choose a set of distorted underwater images to be corrected and enhanced by different methods and then utilize the underwater image quality metrics measurement to evaluate their performance. These original images are shown below.



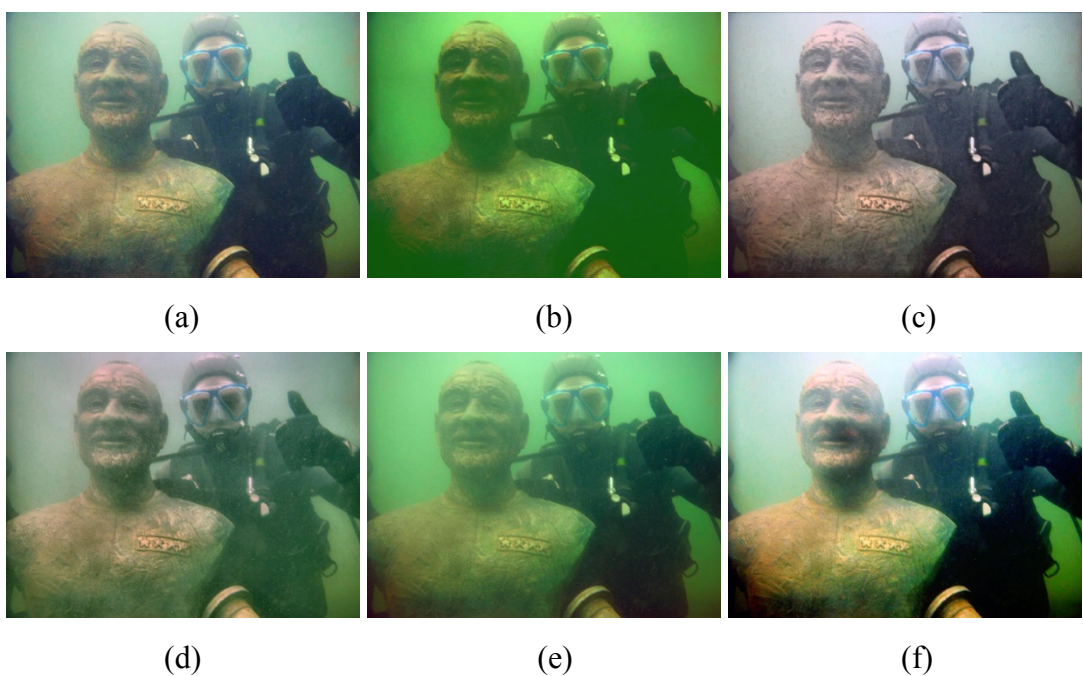
Diver Image (2)

Shoal Image

Shoal Image (2)

Figure 4.16, Another set of images chosen to evaluation and comparison

Firstly, we show the restoration results of different underwater imaging methods, as shown in Figure 4-17, it is obvious that several results perform well for this diver image, the subjective visual performance improves after executing the restoration expect for the histogram equalization (HE) method, which shows poor ability for stretching color dynamic range of original image. Our method achieves great result but the boundary effect tends to be worse than other method, i.e., relatively high information loss in the boundary regions compare to other results.



(a)

(b)

(c)

(d)

(e)

(f)

Figure 4.17, Results on the diver image (2) via different methods. (a) ACE. (b) Histogram equalization (HE). (c) Fu et al. (d) Ancuti et al. (e) Galdran et al. (f) Proposed method.

Despite the subjective visual evaluation method, we also introduce the underwater image quality metrics to evaluate the performance of underwater imaging methods well. The underwater image quality metrics is composed by colorfulness metric, sharpness metric and contrast metric, where colorfulness metric is utilized to measure the color correction performance, sharpness plays a role of reflecting textures and edges of the restored image and contrast metric is used to measure the contrast of restored image.

Since human eyes are more sensitive to low frequency component of an image, where low frequency component reflects the intensity and color of the image, and can not show the small change of high frequency component, which reflects the details and texture information of the image. Based on this case, we find that the visual performance of images has the most influence for determining the image quality, and color casting contributes the most effects to visual performance. So we first analyze the color correction performance of these methods by underwater image colorfulness metric (UICM). As shown in the table 4-5, we compare the mean value and standard deviation of Red-Green (RG) channel and Yellow-Blue (YB) channel, followed by the UICM values. We have mentioned before that an image with good color performance when the μ_{RG} and μ_{YB} are both near to zero, while the contrast is measured by σ_{RG} and σ_{YB} , who should be as large as possible. The μ_{RG} and μ_{YB} of original image is large (-106.74, 61.70) due to the color casting caused by light absorption, where red component attenuates fastest and blue component is absorbed and backscattered by dusk-like particles in this specific water environment, while σ_{RG} and σ_{YB} stay at a low level because of haze. After restoration, Fu et al. achieves the best results in correct the μ_{RG} and μ_{YB} , which is -0.99 and -1.09 separately. They are close to zero. Galdran et al. generates the largest σ_{RG} , while our method gets the highest σ_{YB} . In sum, our method obtains the highest score after computing the UICM value, which means that the proposed method performs best among these algorithms under this measurement standard.

Table 4.5, underwater image colorfulness metric (UICM) results of diver image (2)

<i>Original</i>	<i>ACE</i>	<i>HE</i>	<i>Fu.</i>	<i>Ancuti.</i>	<i>Galdran.</i>	<i>Proposed.</i>
-----------------	------------	-----------	------------	----------------	-----------------	------------------

μ_{RG}	-106.74	-20.89	-66.48	-0.99	-21.90	-45.83	-20.35
μ_{YB}	61.70	5.59	44.56	-1.09	15.21	25.78	9.14
σ_{RG}	13.19	15.38	14.09	10.05	13.62	20.98	18.76
σ_{YB}	11.04	17.48	11.27	12.23	12.52	15.29	24.73
$UICM$	-0.58	3.11	0.72	2.47	2.22	2.71	4.33

Then the underwater image sharpness metric (UISM) and underwater image contrast metric (UIConM) are calculated. The ACE method highest score, 7.06, in UISM measurement, which is closely followed by our method, 7.05. For UIConM measurement, the result of our method stands at the highest level, 0.58, and finally for the comprehensive measurement, underwater image quality metric (UIQM), our method also achieves the highest score. Thus, under this water environment, our method performs best and successfully realizes the color correction and contrast enhancement.

Table 4.6, underwater image quality metric (UIQM) results of diver image (2)

	<i>Original</i>	<i>ACE</i>	<i>HE</i>	<i>Fu.</i>	<i>Ancuti.</i>	<i>Galdran.</i>	<i>Proposed.</i>
<i>UICM</i>	-0.58	3.11	0.72	2.47	2.22	2.71	4.33
<i>UISM</i>	6.96	7.06	6.94	6.84	7.04	6.97	7.05
<i>UIConM</i>	0.34	0.56	0.47	0.51	0.50	0.45	0.58
<i>UIQM</i>	0.26	3.52	1.86	3.91	3.24	2.38	4.28

Below show the restoration results of another type of image, shoal image. From the integral visual performance, the histogram equalization method fails to restore the degraded image, while other five methods successfully correct and enhance the image to some degree.



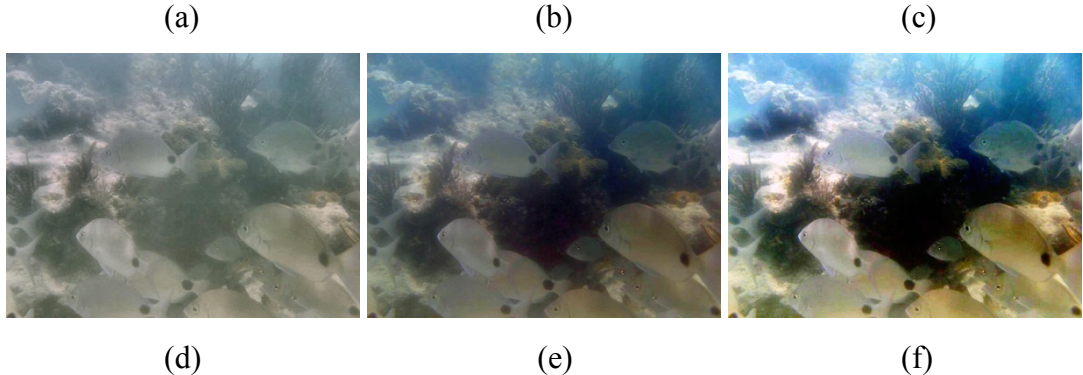


Figure 4.18, Results on the shoal image. (a) ACE. (b) Histogram equalization (HE).
(c) Fu et al. (d) Ancuti et al. (e) Galdran et al. (f) Proposed method.

We can derive from Figure 4-18 that only the restoration result of our method is over-enhancement in the top corner of the image, which causes the image seems unnatural. The result of Ancuti et al. is grayish while Galdran et al. is darkish. Meanwhile, the results of ACE method and Fu et al. show greater performance.

Table 4.7, underwater image colorfulness metric (UICM) results of shoal image

	<i>Original</i>	<i>ACE</i>	<i>HE</i>	<i>Fu.</i>	<i>Ancuti.</i>	<i>Galdran.</i>	<i>Proposed.</i>
μ_{RG}	-43.00	-3.89	-42.87	1.50	-7.83	-9.64	-12.61
μ_{YB}	28.08	-0.23	32.57	0.08	2.46	-7.29	-3.42
σ_{RG}	5.74	12.95	2.24	14.56	6.24	14.17	22.55
σ_{YB}	7.87	18.40	1.70	19.50	10.15	19.10	35.04
<i>UICM</i>	0.17	3.46	-1.00	3.82	1.67	3.45	6.26

Table 4.8, underwater image quality metric (UIQM) results of shoal image

	<i>Original</i>	<i>ACE</i>	<i>HE</i>	<i>Fu.</i>	<i>Ancuti.</i>	<i>Galdran.</i>	<i>Proposed.</i>
<i>UICM</i>	0.17	3.46	-1.00	3.82	1.67	3.45	6.26
<i>UISM</i>	7.09	7.17	5.91	6.81	7.14	7.10	7.05
<i>UICOnM</i>	0.21	0.60	0.09	0.64	0.38	0.48	0.58
<i>UIQM</i>	1.63	4.16	0.84	4.34	3.23	3.53	3.81

In the Table 4.7 and 4.8, we find that although our method achieves greatest performance on colorfulness metric measurements, it fails in the overall evaluation,

where the result of Fu. et al gets the highest UIQM score. And ACE method achieves the best performance in UISM.

We finally put the restoration results among these methods of another shoal image as well as their UICM, UISM, UIConM and UIQM values.

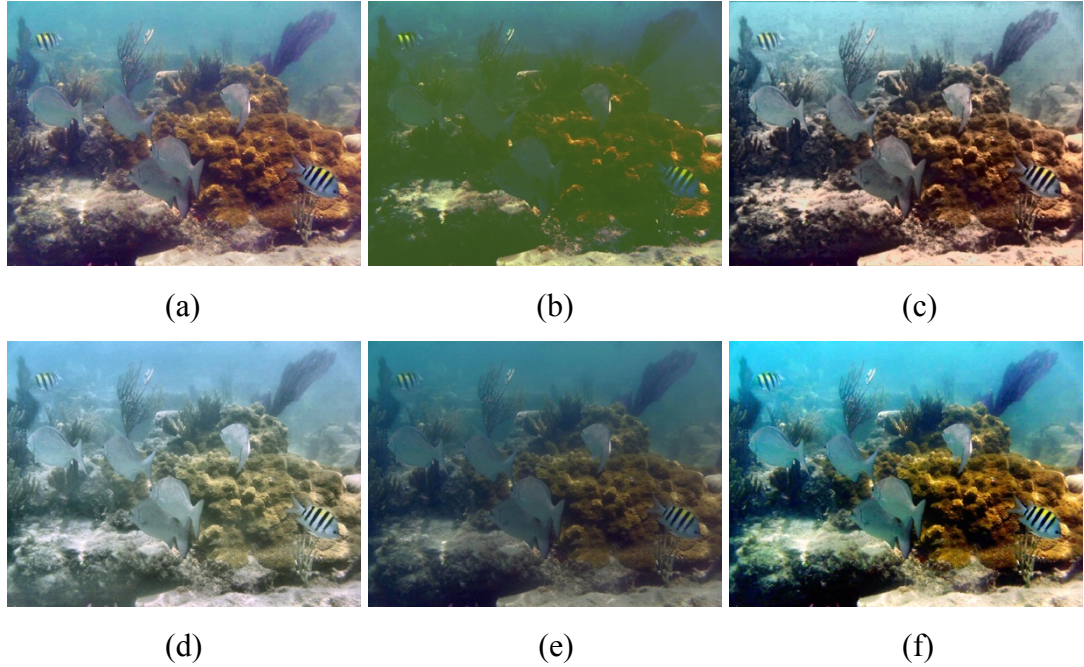


Figure 4.19, Results on the shoal image (2). (a) ACE. (b) Histogram equalization (HE). (c) Fu et al. (d) Ancuti et al. (e) Galdran et al. (f) Proposed method.

Table 4.9, underwater image colorfulness metric (UICM) results of shoal image (2)

	<i>Original</i>	<i>ACE</i>	<i>HE</i>	<i>Fu.</i>	<i>Ancuti.</i>	<i>Galdran.</i>	<i>Proposed.</i>
μ_{RG}	-41.05	-1.46	-27.00	0.63	-23.81	-20.30	-15.99
μ_{YB}	30.15	-12.76	29.20	-2.18	-13.50	-17.26	-17.98
σ_{RG}	13.81	26.60	5.18	25.36	16.36	19.84	41.92
σ_{YB}	12.54	23.70	18.07	22.31	23.03	17.68	41.22
<i>UICM</i>	1.59	5.31	1.92	5.30	3.75	3.50	8.25

Table 4.10, underwater image quality metric (UIQM) results of shoal image (2)

	<i>Original</i>	<i>ACE</i>	<i>HE</i>	<i>Fu.</i>	<i>Ancuti.</i>	<i>Galdran.</i>	<i>Proposed.</i>
<i>UICM</i>	1.59	5.31	1.92	5.30	3.75	3.50	8.25

<i>UISM</i>	6.88	7.05	7.55	6.79	6.90	6.88	7.01
<i>UIConM</i>	0.38	0.69	0.39	0.71	0.61	0.59	0.69
<i>UIQM</i>	3.44	4.70	3.67	4.69	4.32	4.24	4.77

In general, as discussed above, the proposed method successfully solves the issue of underwater objects visibility enhancement. By comparing with the state-of-art methods, we show that our method performs well on various underwater environments. However, the proposed method also has some drawbacks needed to be solved, for instance, it demonstrates the over-enhancement problem for some test images and some information loss exist as well as the boundary effect. Moreover, by introducing different image evaluation techniques, we deal with a comprehensive analysis and evaluation among the results of different methods, then demonstrates the superiorities and good performance of our method.

Chapter 5

Conclusion and Recommendations

5.1 Conclusion

In general, our method is composed of image decomposition process, color correction and dehazing process for two image components separately, then the multi-scale weighted fusion process is utilized to reconstruct the final result. In this thesis, we reviewed several state of the art underwater image enhancement methods and proposed a novel backscatter removing method to enhance the visibility of underwater objects based on the underwater optical model. We then compare the performance of our method with state of the arts by two sets of distorted images captured in the different water environments. Meanwhile, subjective visual evaluation index and several underwater image quality metric measurements are utilized to evaluate and analyze the superiorities and drawbacks.

Our experimental results show the specific features of distorted images captured in the water and the restoration performance of our method as well as other state-of-art methods. Actually, the proposed algorithm generally beats other methods, although some evaluation indexes do not outperform. Among different evaluation indexes and measurements, our method is demonstrated to achieve good performance, in which the performance on dense haze and heavy color casting scenes is even slightly better than the state-of-art algorithms.

5.2 Further work

The proposed underwater image enhancement method is based on underwater optical compensation, image decomposition as well as image fusion technology. The underwater optical model is composed of light absorption and dusk-like particles

backscatter in both vertical direction and horizontal direction, however, in our method, we compensate the attenuation on vertical direction merely use the color constancy method, which may violate the physical process of light propagation. Thus, some limitations exist in our method. For example, our method shows excellent performance for dense haze and heavy color casting underwater images, but the boundary effects are existed which cause the information loss of such areas obviously. Meanwhile, for slight haze and mild color casting situations, our method does not outperform some of the state-of-art methods and even leads over-enhancement for the specific cases. As the gray intensities of each color channel of an image may provide intrinsic information among the physical properties of underwater imaging issue, for future work we will try to find out an efficient way to estimate the vertical depth of arbitrary underwater images and optimize the transmission depth of underwater images more accurate, finally construct the comprehensive, effective and efficient algorithm.

Bibliography

- [1] Chiang J Y, Chen Y C. Underwater image enhancement by wavelength compensation and dehazing[J]. *Image Processing, IEEE Transactions on*, 2012, 21(4): 1756-1769.
- [2] Wang R, Wang Y, Zhang J, et al. Review on underwater image restoration and enhancement algorithms[C]//*Proceedings of the 7th International Conference on Internet Multimedia Computing and Service*. ACM, 2015: 56.
- [3] Schettini R, Corchs S. Underwater image processing: state of the art of restoration and image enhancement methods[J]. *EURASIP Journal on Advances in Signal Processing*, 2010, 2010: 14.
- [4] He K, Sun J, Tang X. Single image haze removal using dark channel prior[J]. *Pattern Analysis and Machine Intelligence, IEEE Transactions on*, 2011, 33(12): 2341-2353.
- [5] Galdran A, Pardo D, Picón A, et al. Automatic Red-Channel underwater image restoration[J]. *Journal of Visual Communication and Image Representation*, 2015, 26: 132-145.
- [6] Chen Z, Wang H, Shen J, et al. Region-specialized underwater image restoration in inhomogeneous optical environments[J]. *Optik-International Journal for Light and Electron Optics*, 2014, 125(9): 2090-2098.
- [7] Lu H, Li Y, Serikawa S. Underwater image enhancement using guided trigonometric bilateral filter and fast automatic color correction[C]//*Image Processing (ICIP), 2013 20th IEEE International Conference on*. IEEE, 2013: 3412-3416.
- [8] Zhao X, Jin T, Qu S. Deriving inherent optical properties from background color and underwater image enhancement[J]. *Ocean Engineering*, 2015, 94: 163-172.
- [9] Van De Weijer J, Gevers T, Gijsenij A. Edge-based color constancy[J]. *Image Processing, IEEE Transactions on*, 2007, 16(9): 2207-2214.
- [10] Buchsbaum G. A spatial processor model for object colour perception[J]. *journal of the Franklin institute*, 1980, 310(1): 1-26.

- [11] Getreuer P. Automatic color enhancement (ACE) and its fast implementation[J]. *Image Processing On Line*, 2012 (2012).
- [12] Limare N, Lisani J L, Morel J M, et al. Simplest color balance[J]. *Image Processing On Line*, 2011, 1.
- [13] Pizer S M, Amburn E P, Austin J D, et al. Adaptive histogram equalization and its variations[J]. *Computer vision, graphics, and image processing*, 1987, 39(3): 355-368.
- [14] Zuiderveld K. Contrast limited adaptive histogram equalization[C]//*Graphics gems IV*. Academic Press Professional, Inc., 1994: 474-485.
- [15] Ancuti C O, Ancuti C, Haber T, et al. Fusion-based restoration of the underwater images[C]//*Image Processing (ICIP)*, 2011 18th IEEE International Conference on. IEEE, 2011: 1557-1560.
- [16] Ancuti C, Ancuti C O, Haber T, et al. Enhancing underwater images and videos by fusion[C]//*Computer Vision and Pattern Recognition (CVPR)*, 2012 IEEE Conference on. IEEE, 2012: 81-88.
- [17] Fu X, Zhuang P, Huang Y, et al. A retinex-based enhancing approach for single underwater image[C]//*Image Processing (ICIP)*, 2014 IEEE International Conference on. IEEE, 2014: 4572-4576.
- [18] Land E H, McCann J. Lightness and retinex theory[J]. *JOSA*, 1971, 61(1): 1-11.
- [19] Ghani A S A, Isa NAM. Underwater image quality enhancement through integrated color model with Rayleigh distribution[J]. *Applied Soft Computing*, 2015, 27: 219-230.
- [20] Ghani A S A, Isa NAM. Enhancement of low quality underwater image through integrated global and local contrast correction[J]. *Applied Soft Computing*, 2015, 37: 332-344.
- [21] Kim J H, Jang W D, Sim J Y, et al. Optimized contrast enhancement for real-time image and video dehazing[J]. *Journal of Visual Communication and Image Representation*, 2013, 24(3): 410-425.
- [22] E. Peli, Contrast in complex images, *J. Opt. Soc. Am. A* 7 (10) (1990) 2032–2040.
- [23] Fattal R. Single image dehazing[C]//*ACM Transactions on Graphics (TOG)*. ACM, 2008, 27(3): 72.

- [24] He K, Sun J, Tang X. Guided image filtering[M]//Computer Vision–ECCV 2010. Springer Berlin Heidelberg, 2010: 1-14.
- [25] Achanta R, Hemami S, Estrada F, et al. Frequency-tuned salient region detection[C]//Computer vision and pattern recognition, 2009. CVPR 2009. IEEE conference on. IEEE, 2009: 1597-1604.
- [26] Jobson D., Rahman Z., Woodell G.A. The statistics of visual representation [J]. Proc. SPIE. 2002, 47(36), 25-35.
- [27] Panetta K, Gao C, Agaian S. Human-Visual-System-Inspired Underwater Image Quality Measures[J].
- [28] J. Bednar and T. L. Watt, “Alpha-trimmed means and their relationship to median filters,” IEEE Trans. Acoust. Speech Signal Process., vol. ASSP-32, no. 1, pp. 145–153, Feb. 1984.